Aerosol particle shrinkage event phenomenology in a South European suburban area during 2009-2015

E. Alonso-Blanco[1], F.J. Gómez-Moreno[1], L. Núñez[1], M. Pujadas[1], M. Cusack[2] and B. Artíñano[1]

[1]Center for Energy, Environmental and Technological Research (CIEMAT), Avenida Complutense 40, 28040 Madrid, Spain
[2]Insitute of Chemical Process Fundamentals of the CAS, v.v.i., Rozvojova 135, 165 02, Prague 6, Czech Republic

Correspondence to: E. Alonso-Blanco (elisabeth.alonso@ciemat.es)

Abstract. A high number of aerosol particle shrinkage cases (70) have been identified and analysed from an extensive and representative database of aerosol size distributions obtained between 2009 and 2015 at an urban background site in Madrid (Spain).

A descriptive classification based on the process from which the shrinkage began is proposed according which shrinkage events were divided into three groups: (1) NPF+shrinkage (NPF+S) events, (2) aerosol particle growth process+shrinkage (G+S) events, and (3) pure shrinkage (S) events.

The largest number of shrinkages corresponded to the S-type followed by NPF+S, while the G+S events were the least frequent group recorded. Duration of shrinkages varied widely from 0.75 to 8.5 h and SR from -1.0 to -11.1 nm $\cdot h^{-1}$.

These processes typically occurred in the afternoon, around 18:00 UTC, caused by two situations: i) a wind speed increase usually associated with a change in the wind direction (over 60% of the observations) and ii) the reduction of photochemical activity at the end of the day.

All shrinkages were detected during the warm period, mainly between May and August, when local meteorological conditions (high solar irradiance and temperature and low relative humidity), atmospheric processes (high photochemical activity) and availability of aerosol-forming precursors were favorable for their development.

As a consequence of these processes, the particles concentration corresponding to the Aitken mode decreased into the nucleation mode. The accumulation mode did not undergo significant changes during these processes. In some cases, a dilution of the particulate content in the ambient air was observed.

This work, goes further than others works dealing with aerosol particles shrinkages, as it incorporates as a main novelty a classification methodology for studying these processes. Moreover, compared to other studies, it is supported by a high and representative number of observations. Thus this study contributes to get a better understanding of these types of atmospheric aerosol transformations and its features.

Keywords: Aerosol particle shrinkage events, Aerosol particle size, Aerosol dynamics, Aerosol size distribution, New particle formation, Scanning mobility particle sizer.

1. Introduction

Studies focused on atmospheric particle size diminution are becoming usual in recent scientific literature. Different terms have been used to name this process, as shrunken particle size (Yao et al., 2010), aerosol particle growth reversals (Yao et al., 2010;Skrabalova et al., 2015) or shrinkage (Young et al., 2013;Cusack et al., 2013;Skrabalova et al., 2015;Salma et al., 2016b;Lihavainen et al., 2016;Neitola et al., 2014), the latter being the most commonly used. The most complete definition has possibly been enunciated by Young et al. (2013). This author first described ~~who first described~~ the fundamental condition of this process, that is, the decrease in particle size caused by particle-to-gas conversion having a sufficient duration that allows for its observation (for Young et al. (2013) ~2 h).

Atmospheric aerosol shrinkages have been observed in geographically disparate locations around the world and, therefore, under differing climatic conditions. On the Asian continent, Yao et al. (2010) documented these processes at a coastal suburban site and Young et al. (2013) observed shrinkage processes at a coastal, urban and downwind site, with both sites being subtropical climate sites. On the American continent, Backman et al. (2012) detected these processes at an urban background site also in a subtropical climate. In Europe, Cusack et al. (2013) studied these processes at a regional background site with a Mediterranean climate, Skrabalova et al. (2015) identified shrinkage processes at an urban background station in a continental climate and Neitola et al. (2014) and Lihavainen et al. (2016) observed these processes at a rural background site with an arid climate. Nonetheless, the number of cases identified in these studies has not been particularly numerous relative to the duration of the measurement period involved (either short field campaigns or continuous measurements). Out of these only three

works exceed a year of measurements, presenting a variable number of cases identified; Salma et al. (2016b) observed 8 cases in 36 months of measurements, Skrabalova et al. (2015) 22 cases in 24 months and Yao et al. (2010) 2 cases in 12 months.

Most of these authors noticed aerosol particle shrinkages during the growth phase of newly nucleated particles (Yao et al., 2010;Young et al., 2013;Cusack et al., 2013;Skrabalova et al., 2015;Neitola et al., 2014), whereas some authors exceptionally documented them in the absence of new particle formation (NPF) (Cusack et al., 2013;Backman et al., 2012). But as general rule, all these processes appear to be depending, in a highly complex way, on ambient and meteorological parameters. In this sense, two aspects emerge as fundamental variables; the aerosol nature (secondary organic aerosols) and ambient conditions such as wind speed, air temperature or photochemical activity. With regard to aerosol nature, the volatile fraction of the aerosols involved in these processes is very high (Kecorius et al., 2015), although the characteristics of the condensable organic matter taking part in the process is still an open question. With regard to ambient conditions, meteorological factors control the gas-particle partitioning of vapors in order to maintain the balance between them as mentioned by Robinson et al. (2007) from laboratory studies.

There are several reasons why these processes are under investigation. In the atmosphere, aerosol shrinkage dynamics is highly complex. The reactive chemistry that governs these processes implies particle transformations that affect both the aerosol composition and the size distribution and consequently their behavior in the atmosphere. Thus, the study of these phenomena can help to improve the understanding of aerosol dynamics under real atmospheric conditions. In addition, changes in the particle size during these processes, towards smaller particle sizes, have implications for climate (IPCC, 2013), air quality and human health (Harrison and Yin, 2000;Donaldson et al., 2001). For example, the light scattering per unit mass produced by small particles is higher than by larger ones, which has consequent effects on climate–aerosol interactions (Seinfeld and Pandis, 2016) and also on visibility (Charlson, 1969;Watson, 2002). Likewise, in relation to human health implications, smaller particle sizes are more readily incorporated and absorbed into the human body (Oberdörster et al., 2005). In addition, this phenomenon can be considered of exceptional interest because of its uniqueness, and therefore, the processes which lead to their development are still a matter of study.

This paper has two main objectives: i) identify and classify the shrinkage processes based on a easily-applicable methodology and ii) explore the possible causes that trigger aerosol particle shrinkages at an urban background site located in the urban area of Madrid (Spain). To accomplish these objectives an exhaustive study of a 6.5 year time-series of aerosol size distribution measurements has been conducted. Firstly, shrinkage events have been identified according to different parameters such as the total (N_{tot}) and modal (N_{nuc}, N_{Ait} and N_{acc}) particle number concentrations, the aerosol size distribution and the estimation of the growth and shrinkage rates in relation to air mass composition and meteorological variables. Subsequently, the cases identified have been categorized with respect to the aerosol processes which preceded the shrinkage ones. Finally, the possible causes that lead to the beginning of the shrinkage have been analyzed and discussed in this work.

2. Methodology

2.1 Site description and measurements

The experimental site (40° 25′ 08″ North, 3° 41′ 31″ West and 657 m asl) is located at the facilities of the Center for Energy, Environmental and Technological Research (CIEMAT) (Fig. 1), approximately 9 km north-northwest of Madrid city center. The site is surrounded by three large natural areas: Dehesa de la Villa Park (a few hundred meters east), Casa de Campo Park (approximately 7.5~~0~~ km Southwest) and the Monte del Pardo forest area (approximately 22 km Northwest). In addition, at a distance of 1-2 km to the west is the M30 motorway, the main overhead highway in Madrid with a traffic intensity on average ~ 300,000 vehicles per day. The area can be classified as an urban background site since it is not directly influenced by traffic emission sources.

Madrid is the most populous Spanish city with more than 3 million inhabitants. That number increases to 6 million when the metropolitan area is considered. Situated in the center of the Iberian Peninsula, the city is the focal point of the national highway system. Thus, with a light industry, atmospheric emissions from traffic and heating devices are the main contributors to the aerosol fine fraction, especially in winter time (Salvador et al., 2012;Salvador, 2004;Gómez-Moreno et al., 2011).

Local Climate is Continental-Mediterranean influenced by urban features. The wind regional circulation in the Madrid Basin is controlled by the Central Mountain

System located some 50-70 kilometers north-northwest of the city, responding to mountain breezes.

For this study and due to the complexity of the processes to be analyzed an important number of variables have been considered, i.e. aerosol properties, pollutant gases and meteorological conditions. These data have been obtained by a variety of instruments at the CIEMAT site between July 2009 and December 2015. A brief description of the measurements and instrumentation is included below:

- Particle number size distributions: a scanning mobility particle sizer (TSI-SMPS model 3936), consisting of an electrostatic classifier (EC; TSI Inc., model 3080), a differential mobility analyzer (DMA; TSI Inc., Model 3081) and a condensation particle counter (CPC; TSI Inc., model 3775) provided continuous measurements of the submicrometer particle size range from 14.6 to 661.2 nm, divided into 107 size bins. The particles were measured under dry conditions (RH<40%), in accordance with the ACTRIS (Aerosols, Clouds, and Trace gases Research Infrastructure Network) SMPS standards (Wiedensohler et al., 2012). The precision of the SMPS system has been checked during the intercomparison campaigns performed within the framework of the Spanish Network on Environmental DMAs (REDMAAS: http://www.redmaas.com/) (Gómez-Moreno et al., 2010;Gómez-Moreno et al., 2015;Gómez-Moreno et al., 2016). During these campaigns, the flow rates and the DMA voltage were verified and the SMPS was calibrated with polystyrene latex (PSL) particles. After this common checking, the CPC and the SMPS were intercompared with other instruments to test the representativeness of their measurements over time. Data acquisition with a temporal resolution of 4.5 minutes was done by TSI Aerosol Instrument Manager (AIM). Figure 2 shows the data coverage for aerosol size distribution, core of the measurements used in this study. Data gaps were mainly due to regular calibration of the measurement systems or breakdowns. As special fact, it is important to point out that SMPS technical problems did not allow us using the data of the first nine channels from June to December 2012. 68% of the data was available for the entire measurement period. With the exception of the years 2009 and 2014, more than 50% of the SMPS data were available yearly with an intra-annual distribution varying from 55% (2010) to 83% (2012).

- Air mass composition: concentrations of trace gases such as NO, NO_2 and O_3 were provided by a differential optical absorption spectrometer (DOAS OPSIS AR-500) (Platt and Stutz, 2008). The DOAS system employed a defined absorption path of 228 meters length at an average height of 10 m agl. The equipment offers an approximately 7-minute analysis cycle for all species measured. Calibrations have been performed with cells and reference gases to ensure the proper functioning of the equipment and data quality.

  Air pollutants were completed with representative observations obtained at the Casa de Campo monitoring station (3º 44' 50.44'' West, 40º 25' 09.68'' North, 645 m asl). This station, about 4.5 km southwest of CIEMAT, is one of 24 automatic stations belonging to the Air Quality Monitoring Network of the Madrid municipality. Hourly levels of SO_2, NO_x and O_3 are provided by this station, thus complementing the data obtained by the DOAS system.

- Meteorology: meteorological parameters have been measured at a three-level instrumented tower 55 m high, averaged and recorded automatically with a 10-minute frequency. Atmospheric pressure is acquired at ground level, temperature and relative humidity at level 1 (4 m agl), solar irradiance and precipitation at level 2 (35 m agl) and finally, wind speed and direction at the top level, level 3 (55 m agl). The different meteorological sensors are calibrated semi-annually.

- Synoptic meteorology and air masses origin: atmospheric synoptic situation has been analyzed using synoptic charts at two levels, 700 (~ 3000 m above msl) and 850 mb (~1500 m above msl), compiled from the UK's national meteorological service (Met Office: http://www.metoffice.gov.uk/) and the German Meteorological Service (http://www.wetterzentrale.de/) for those days in which shrinkage events were identified. Furthermore, results of the NOAA-HYSPLIT air mass back-trajectory model (Stein et al., 2015;Rolph, 2016) have been considered to identify the air masses origin arriving at CIEMAT. To that end, 24-h backward trajectories ending before and at the onset of the shrinkage processes have been calculated at 100, 500 m and 1000 m agl.

2.2. Shrinkage event identification

In this study, the term "shrinkage event" will be presented as the sum of the process that precedes the shrinkage (NPF or aerosol particle growth process) and the shrinkage process itself, which have been naming in this study as phases of the event.

A first approximation of the identification of these events has been done by the visual method of day-to-day as proposed by Dal Maso et al. (2005) for the detection of NPF episodes. Thus, daily (24-h) surface plots on aerosol size distributions have been produced and inspected. Subsequently, following identification of potential shrinkage events, different parameters were incorporated into the analysis to discard those "apparent shrinkages".

The aerosol size distribution shape was evaluated to detect sudden changes that did not respond to the expected dynamics of the processes involved during shrinkage events. In addition, the measured particle mode diameter (D_{mode}) was calculated for 15-min average aerosol size distributions using log-normal fits to estimate modal growth/shrinkage rate (GR/SR). Notation was according to the equation GR (in positive (+) value) or SR (in negative (-) value)=$\Delta D_{mode}/\Delta t$ used in Kulmala et al. (2012). For modal particle size below 14.6 nm (below the detection limit of the SMPS), i.e. in the initial stage of nucleation, it was not possible to estimate D_{mode}.

The evolution of the total number of particles (N_{tot}=particles number concentration between 14.6 and 661.2 nm) and the modal number concentrations, nucleation (N_{nuc}=particles number conc. between 14.6 and 30 nm), Aitken (N_{Ait}= particles number conc. between 30 and 100 nm) and accumulation (N_{acc}=particles number conc. between 100 and 661.2 nm), from the aerosol size distributions have also been calculated. These parameters are important to quantify the transformation processes of the particles and the subsequent effect on the particle number concentration. Both the changes observed among the modal particle-size fractions (N_{nuc}, N_{Ait}, and N_{acc}) and the evolution of GR and SR facilitate the identification of shrinkage processes.

The air masses characteristics and their variations during the shrinkage events have also been studied at the sampling point. For this purpose, trace gases concentrations, meteorological data, synoptic charts and air mass back-trajectories have been used. Here, the dilution processes of atmospheric aerosol have also been evaluated. Due to the physical aerosol particle changes occurring during the processes studied,

aerosol particle dilution has been considered when the difference in ~~particle~~ their concentration between the two phases of the event (NPF or aerosol particle growth phase vs shrinkage phase) is greater than 10%.

Additionally, as it has become clear in previous investigations on aerosol particle shrinkage, NPF plays an important role in these processes. Therefore it has been necessary to incorporate in this work some parameters such as the aerosol condensation sink and the gas-phase H_2SO_4 proxy value.

The aerosol condensation sink (CS) is considered a metric for measuring the scavenging speed of atmospheric molecules by condensation onto pre-existing aerosol particle (Pirjola et al., 1999;Lehtinen et al., 2003). This parameter has been calculated from the aerosol size distribution data according to Lehtinen et al. (2003) using the following equation:

$$CS = 2\pi D \sum_i^0 \beta_{M.i} d_{p_i} N_i \quad (1)$$

where D is the diffusion coefficient of the condensing vapor in the gas phase (in this study assumed that D is the H_2SO_4 diffusion coefficient, 0.104 $cm^2 \cdot s^{-1}$ (Lyman et al., 1990)), $\beta_{M.i}$ is the transitional correction factor (Fuchs and Sutugin, 1971), d_{p_i} is the particle diameter and N_i (cm^{-3}) is the particle number concentration for each particle size discrete interval i.

Since CS depends strongly on the particles size distribution, i.e. the particle concentration and their sizes, their temporal variations are similar (see Fig. S1-S3).

NPF typically appears jointly with a low condensation sink values, ~~in other words,~~ i.e. when the pre-existing aerosol particle concentration in the atmosphere is low, thus promoting gas-to-particle conversion.

The conversion of SO_2 into H_2SO_4 was calculated according to the universal formulation of the [H_2SO_4] proxy developed by Mikkonen et al. (2011). This non-linear proxy has been constructed based on measurements of gases ([H_2SO_4], [SO_2] and [O_3]), meteorological parameters (relative humidity, temperature and radiation) and aerosol size distribution collected at six sites in Europe and North America, among them five rural areas and one urban area. SO_2 is required as a precursor for sulfuric acid (Seinfeld and Pandis, 2016) which seems to be the one of the most important factors that governs both particle nucleation and growth as numerous studies have found (Kusaka et al.,

1998;Kulmala et al., 2000;Kulmala and Laaksonen, 1990). The SO_2 measured in the study area is originated mainly from road traffic. Thus, SO_2 concentration varied from 1 to 14 $\mu g \cdot m^{-3}$ depending on the traffic emissions.

The H_2SO_4 proxy concentration is obtained by the equation (2) included below:

$$[H_2SO_4] = 8.21 \times 10^{-13} \, \kappa \, Radiation \, [SO_2]^{0.62} \, (CS \; RH)^{-0.13} \quad (2)$$

where κ is the temperature-dependent reaction rate constant, which is calculated according to Eq. (3) in Mikkonen et al. (2011), and is scaled by multiplying it with 10^{12} ($m^2 \cdot W^{-1} s^{-1}$), $Radiation$ is the global solar radiation ($W \cdot m^{-2}$), $[SO_2]$ is the measured SO_2 concentrations ·(molecules ·cm^{-3}), CS is the condensation sink (s^{-1}), and RH is the relative humidity (%).

The reason to present here the [H_2SO_4] results using the general approach of Mikkonen is because none of all the sites considered by Mikkonen et al. (2011) fits to the features of the CIEMAT site, neither in emission sources, nor land uses or meteorological conditions. This equation has not been tested against sulfuric acid data for urban environments comparable to CIEMAT. However, it has been used in numerous studies, among them, some focused on urban areas (Xiao et al., 2015;Yu et al., 2016;Siakavaras et al., 2016;Kontkanen et al., 2017), reporting similar values to this study. Given that the real chemical process seem to be covered in the Mikkonen's equation (Seinfeld and Pandis, 2016), this proxy has been applied in this work as a tool to predict the ambient [H_2SO_4] concentrations at the site.

Recent studies on NPF suggests that the highly oxygenated molecules (HOMs), including the extremely low-volatile organic compounds (ELVOCs), take part, together with H_2SO_4, in the nucleation process (Kulmala et al., 2014;Bianchi et al., 2016;Ehn et al., 2014;Ehn et al., 2012). These studies, mostly limited to laboratory experiments, have proven the important role of very low volatility biogenic vapors as precursors of aerosol formation (Kirkby et al., 2016;Tröstl et al., 2016;Ehn et al., 2014). Indeed, some authors have found this link under atmospheric conditions (Vogel et al., 2016;Bianchi et al., 2016). A previous NPF study at this site (Gómez-Moreno et al., 2011) goes along these lines. The organic vapors, especially those of biogenic origin from regional emissions, seem to be critical in the aerosol particles formation in the study area.

Given the lack of existing classification method on shrinkage processes, a descriptive classification has been proposed for their study here based on the process that precede their development. The detailed analysis of the different parameters considered in this investigation has made possible to classify the identified shrinkage events into three different groups (fig. 3):

(1) NPF+shrinkage (NPF+S) events: this group of shrinkages occurs after the growth of nucleated particles of class I (Dal Maso et al., 2005), both of subclass Ia and Ib. These NPF subclasses present a typical banana-shaped growth profile, well-formed in Ia but less pronounced in Ib.

(2) Aerosol particle growth process+shrinkage (G+S) events: in such cases where the decrease of particle size happens subsequently to a growth process are classified as G+S events. In these cases ~~particle~~ atmospheric nucleation does not take place.

(3) Pure shrinkage (S) events: shrinkage process only, whereby there is not any previous process occurring.

According to the classification criterion, beyond the three groups of shrinkages identified in this study none other can exist for the database analyzed. The duration of the shrinkage phase has not been considered for the proposed classification.

An example of each shrinkage group can be seen in the figure 3. The time evolution of the size distribution of aerosol particles on surface plots, the D_{mode} and 1-h average aerosol size distributions have been represented for each phase. The first surface plot (1) shows an NPF+S event where the growth phase from small particle sizes and its further shrinkage phase are observed. In the second surface plot (2) both growth and shrinkages phase are measured, the particle growth starting from larger particles sizes, and finally in the last plot (3) only the shrinkage phase was recorded.

3. Results and Discussion

3.1. Overview of the observed aerosol particle shrinkage cases

A total of 70 cases were identified from a SMPS dataset of around 1600 days, all of which have been detected during the warm seasons (spring and summer), when the following necessary conditions are met. On the one hand, changes in ambient conditions

such as an increase in temperature and solar irradiance during daylight hours lead to an increase in the production of biogenic emissions. Thus, availability aerosol-forming precursors and an increase in photochemical reactions in the presence of intensified UV radiation promote the atmospheric aerosol formation. On the other hand, regional air flows and recirculation processes in the study area prolong the aerosol lifetime in the atmosphere which allows for the observation of both its formation and transformation over time. Evidence of this was observed for a number of days studied, in which two or more processes (NPF, aerosol particle growth process or shrinkage process) often occurred. The situation observed at the CIEMAT site is not exceptional, as this types of processes have been identified mainly under temperate climates during the warm seasons in all previous aforementioned studies, with the exception of events described by Skrabalova et al. (2015) and Salma et al. (2016b) which occurred under cold climates (Table 1).

The occurrence and time distribution differences varied from year to year for the period studied, from 21 cases in 2010 to 4 in 2011 as shown in table 2. The scarce number of events identified in 2011 was attributed to the lack of data coverage (54 % of the data during the warm period).

Up to 97% of the events were recorded in May, June, July and August. Exceptionally two events were identified out of this period, one in April 2013 and another in September 2015. The monthly distribution of shrinkage events during the study period is presented in table 2. No apparent cause was found for the variation in shrinkage events occurrence.

A comprehensive analysis of meteorological observations for the four years studied (2010, 2012, 2013 and 2015), in which the availability of warm season data exceeded 70% coverage, was made in order to identify the possible causes of the shrinkage phenomenon.

The inter-annual variation of shrinkage events are in agreement with variations from the norm of the temperature and precipitation relative to regular climatic conditions provided by the Spanish National Agency for Meteorology (AEMET). The variations of the average annual temperature in relation to normal climatological values seem to negatively correlate to the number of annual cases. In contrast, total annual precipitation was positively correlated with the frequency of events. R^2 was found to be ~ 0.7 in both parameters. These meteorological anomalies in relation to the

climatological normal values observed may be conditioning the temporal variations of biogenic vapors and therefore the observations of shrinkages at the site.

In addition, the synoptic weather situation at the surface level have been analyzed in those days when the shrinkage events occurred as well as the 24-h air mass back trajectories from 3 different altitude levels (100, 500 and 1000 m agl) during their course and no pattern has been observed.

3.2. Characteristics of aerosol particle shrinkage events

The total number (70 cases) of aerosol particle shrinkage events was grouped according to the descriptive classification proposed in this work. 30 of the documented events corresponded to pure shrinkage (S) group, 28 to NPF+shrinkage (NPF+S), and the rest, 12 cases in total, belonging to the aerosol particle growth process+shrinkage (G+S) group. A summary of the cases categorized in each of the three groups can be found in tables ~~3~~S1, ~~4~~ S2 and ~~5~~ S3. To date a total of 40 cases have been reported in the literature, the sum of which is still significantly lower than the sum of all cases identified in this study. Out of these, two corresponded to the S group (Backman et al., 2012;Cusack et al., 2013) and the remaining cases to the NPF+S group (Young et al., 2013;Yao et al., 2010;Salma et al., 2016b;Cusack et al., 2013;Skrabalova et al., 2015;Lihavainen et al., 2016).

NPF+S events were observed on clean days marked with low background ~~levels~~ pollutant levels. On such days, the emergence of NPF occurred around 12:00 UTC (fig. 4), under low CS values (taking into account the 28 cases, the average CS was $7.6 \times 10^{-3} \pm 4.2 \times 10^{-3}$ for the preceding two hours to the NPF phase vs $8.9 \times 10^{-3} \pm 3.7 \times 10^{-3}$ s^{-1} preceding the shrinkage phase). The optimal meteorological conditions during the NPF phase (time of maximum solar irradiance, high temperature and low relative humidity (Hamed et al., 2011) (698±119 W m^{-2}, 26±5 ^{o}C and 24±7%, respectively, average values for the 28 cases) led to an increase in photochemical transformations (causing high ozone concentrations and availability of H_2SO_4).

The wind circulation also appeared to have an important influence on the NPF episodes (Gómez-Moreno et al., 2011). The variations of the wind direction in the study region draw a NE-SW main directional axis. During the nocturnal period, NE flows are generated (21:00-08:00 UTC (Local time = UTC+2 hours)). From sun rise to noon, as the air masses are heated on mountain slopes, the flows turn in a clockwise direction from NE to SW (09:00-20:00 UTC), that is maintained until nightfall (Salvador et al.,

2004;Pujadas et al., 2000;Plaza and Artíñano, 1994;Artíñano et al., 2003;Artíñano et al., 1994). When the NPF episodes are observed (~12:00 UTC), the wind direction data indicated an air mass flow from the West (El Pardo forest area) and Southwest (Casa de Campo Park). This suggested a direct transport of biogenic organic emissions towards the sampling site. The NPF phase ranged between 4.25 and 11.25 h with GR oscillating between 1.4 and 10.6 nm $\cdot h^{-1}$. The shrinkage phase began at about 18:00 UTC (fig. 4) with an average duration less than the NPF phase, 3.1±1.4 vs 6.7±1.9 h and a SR ranging from -1.5 to -10.2 nm $\cdot h^{-1}$. This type of event has been the only one for where several consecutive phases of aerosol particle growth and shrinkage processes were noticed (see table 1). Although it is difficult to make comparisons with others studies, given the great diversity of cases of NPF+S events found in the literature, the rates reported from the different investigations (Table 1), are in line with those found in this investigation. Two examples of a shrinkage process associated with NPF are shown in fig. S1.

An important point in agreement with some of the studies reported in Table 1 is the close links between NPF episodes and shrinkage processes (28 NPF+S events out of 70 cases). Thus, as some studies have confirmed the NPF occurrence at regional scale (Salma et al., 2016a;Kim et al., 2016), the NPF+S events will probably take place at the same scale, although this fact has not been confirmed yet.

A group of events not previously described in the literature are the shrinkages occurring during the aerosol particle growth process in the absence of NPF, the so called G+S events. These events have been observed under two well-differentiated situations. A first subgroup of G+S events (3 observations) was detected at midday (around 12:00 UTC) (Fig. 4) under calm conditions (~2 m $\cdot s^{-1}$). This subgroup of events is conditioned by the emissions pattern typical of the study area. The total particle number concentration showed three peaks during spring and summer; two of them associated with traffic emission (in the morning and afternoon) and a third at midday due to the formation of particles by photochemical nucleation processes (Gómez-Moreno et al., 2011). The arrival of polluted air by aerosol particles from traffic emissions during the early morning hours (~ 07:00 UTC) at this experimental site limited the NPF episodes. CS values both for the previous two hours to the growth phase and for growth phase was ~1.45 $x10^{-3}$ s^{-1}.

In addition, during the growth phase, the prevailing winds from the green areas close to the site suggested the transport of biogenic volatile organic emissions to the

410 sampling site. Although new particle formation did not occur, the condensable vapors
411 transported to the site may have participated in particles growth process, reaching an
412 average GR of 5.5±1.0 nm·h^{-1}. Figure S2A shows an example of a case of this first
413 subgroup of G+S event.

414 A second subgroup of cases (9 observations) was noted late afternoon. These
415 shrinkage processes were observed during the recirculation of polluted air by traffic
416 emissions (NO and NO_2 values are elevated during this period) (Fig. S2B), a situation
417 already characterized in the study area (Gómez-Moreno et al., 2011;Pujadas et al., 2000)
418 as revealed wind direction observations (around NE sector). Although it is not quite so
419 common, this second subgroup has also been found under air masses free of traffic
420 emissions, possibly associated with biogenic secondary organic aerosol particle
421 transport from the vegetated areas close to CIEMAT (Fig. S2C). Both types of air masses
422 generally contain a higher concentration of condensable gases, thus the particles grew
423 rapidly (GR of 4.9±1.9 nm·h^{-1}) for a short period (over 1.5 hours). In both subgroups the
424 shrinkage was observed from 18:00 UTC onwards. However, the shrinkage phases for
425 the first subgroup were longer lasting and with a SR lower than the second subgroup,
426 3.7±2.3 h and -2.7±0.5 nm·h^{-1} vs 2.7±1.2 h and -4.9±1.5 nm·h^{-1} respectively.

427 Pure shrinkage processes (S events) were mostly recorded during the afternoon
428 (Fig. 4). These events occurred both under polluted and clean air masses (Fig. S3), i.e.
429 from secondary aerosol particles of anthropogenic (Fig. S3A), and biogenic origin (Fig.
430 S3B) respectively. In the first situation, at first hours, the air masses come mainly from a
431 sector centered on NE, resulting in an increase in NO and NO_2 concentrations associated
432 with a reduction of the O_3 concentration (oxidation of NO by ozone) at the site. In the
433 second situation, in the same period, the winds arrived at the site from the close densely
434 vegetated areas located in the NW sector and any NOx increasing was not observed. The
435 shrinkage phase in this type of event had the longest duration recorded for all shrinkage
436 events in this study (between 1.45 to 8.5 h) with a mean SR of -4.8±3.2 nm·h^{-1}.

437 As already stated above, shrinkage processes mostly tended to start in the late
438 afternoon, around 18:00 UTC. This contrasts with findings of most of the previous
439 investigations on shrinkages (Table 1), where these processes were recorded around
440 midday. Only one of these studies identified these processes in the afternoon, in this case
441 during NPF episodes (Lihavainen et al., 2016).

Except for those of Cusack et al. (2013) and Lihavainen et al. (2016), all cases have occurred in measurement areas with a clear influence of anthropogenic emissions. Nevertheless, these processes have been described in relation to biogenic secondary organic aerosol (mainly NPF episodes), and have not considered the influence of secondary organic aerosol formed from anthropogenic precursors. Here, in contrast to those studies, both the influence of biogenic and anthropogenic secondary organic aerosol has been discussed. This fact highlights how important ambient atmospheric conditions are in the triggering of shrinkage events in measurement area, as will be described in the following section.

3.3. Analysis of shrinkage causes and effects on particle concentrations and size distributions

Atmospheric dilution seems to be the main cause of the aerosol particle shrinkage processes, probably owing to the loss of their volatile fraction. 54% of documented cases were identified under a wind speed increase (>25%) during the shrinkage phase in relation to the previous phase (for NPF+S and G+S events) or the two precedent hours (for shrinkage events). Nearly half of the cases were identified under winds coming from a NE direction. For the events classified as S group, ~~wind~~ atmospheric dilution was the main driver of this process, with 28 of the 30 cases observed under wind speeds > 4 m $\cdot s^{-1}$ (up to 8.7 m $\cdot s^{-1}$). Photochemical activity also played an important role in some of the observations, especially in the NPF+S and G+S events. The decrease in photochemical activity during the final part of the day led to a lower production of gaseous precursors and suppressed the formation of low-volatility products in the atmosphere. The absence of aerosol-forming precursors in the atmosphere makes particle growth by condensation mechanisms difficult. For these cases, the SR seemed to be slower than those majority shrinkages were caused by wind conditions, -3.6±1.6 vs -4.7±2.6 nm $\cdot h^{-1}$ (with wind speed <4 m $\cdot s^{-1}$ and >4 m $\cdot s^{-1}$ during the shrinkage phase, respectively). As Backman et al. (2012) and Skrabalova et al. (2015) point out, this confirms wind speed is the more effective factor in the development of these processes.

Some authors as Salma et al. (2016b), Young et al. (2013) and Yao et al. (2010) ~~also~~ point at atmospheric dilution and air temperature as the two main drivers of these processes. In the absence of prior processes, shrinkage events have only been reported as a result of the evaporation of organic vapors at high ambient temperatures (Backman et al., 2012;Cusack et al., 2013). In this investigation temperature did not appear to be a

475 decisive feature in the development of these processes. Exceptionally, Yao et al. (2010)
476 and Skrabalova et al. (2015) proposed a decrease in the photochemical oxidation as a
477 possible cause, which we have also identified as an important factor in the development
478 of the shrinkages events.

479 The aerosol particles structural changes produced by water uptake or
480 evaporation have been discarded as cause of aerosol particles shrinkage in this study by
481 two main reasons. On the one hand, aerosol particles shrinkages were only observed in
482 the warm period, hot and dry in these latitudes. The ambient RH rarely was over 40 %
483 during these processes (see Tables S1-S3). In addition, the atmospheric particle sampling
484 was conditioned by a nafion dryer. SMPS measurements obtained above 40% RH are
485 considered invalid according ACTRIS standards for SMPS. On the other hand, the
486 hygroscopicity measurements (at 90% RH) obtained at this site have shown that the
487 particles associated to the traffic emissions have a low hygroscopicity (Alonso-Blanco et
488 al., 2014), as it corresponds to particles with high content in organics. Similar findings
489 have also been observed during NPF episodes although these results will be discussed
490 in a future article.

491 These meteorological conditions led to aerosol transformations which affect the
492 size distribution of airborne particles and consequently, the particle concentration
493 corresponding to each mode, characteristic features of the NPF, growth and shrinkage
494 processes. Size distributions results of aerosol particle number concentration revealed
495 the dynamics of these processes. Typically, during the particle formation and growth,
496 the aerosol particle size distribution showed a unimodal shape which underwent a
497 gradual shift towards larger sizes. In contrast, during the shrinkage phase the
498 displacement turned towards smaller sizes as a result of the losses of organic vapors
499 from the aerosol particles. In this last phase the aerosol particle size distribution
500 remained in a unimodal shaped (Fig. 3). Exceptionally, in some observations a bimodal
501 size distribution was observed throughout the event (table S2).

502 Consequently, nucleation and Aitken modes suffered the greatest changes, in
503 contrast to the accumulation mode which hardly varied throughout these events. An
504 example of the typical evolution of the total particle concentration and modal
505 distribution for each identified shrinkage group can be seen in fig. 5. During the NPF
506 episodes the newly formed particles grow rapidly into the Aitken mode sizes. Similar
507 behavior has also been described in previous studies concerning NPF (Cusack et al.,

2013;Yao et al., 2010;Young et al., 2013;Vehkamäki et al., 2004). Conversely, during the shrinkage processes a displacement of particle concentrations towards smaller sizes (N_{nuc}) was observed. During the growth phase, the changes between the concentrations of nucleation and Aitken modes were not so evident and mainly corresponded to the Aitken mode. The latter situation has also been found for some shrinkage processes in this study.

In some cases when shrinkage process was mainly associated to a wind speed increase, the particle concentration suffered variations as a result of the dilution effect. Particle losses of over 30% (number of particles) were observed under wind speeds up to 2 times higher during the shrinkage phase than during the previous phase.

5. Conclusions

A continuous 6.5 year long time series of SMPS observations was analyzed to identify aerosol particle shrinkage processes. 70 cases were detected and documented, being the most exhaustive study on this kind of phenomena from those reported in the literature. This high number of cases has allowed us to develop a classification of these processes based on their main characteristics. In particular, the environmental conditions that exist in the area before the occurrence of aerosol particle shrinkage processes have been considered key factors in that classification.

All the shrinkage processes took place during the warm seasons (spring and summer), mostly in May, June, July and August, when the optimal conditions for their development occur. In this period, the meteorological conditions (high temperature and insolation and low RH), are also favorable to the occurrence of photochemical transformations and vegetation biological activity with high BVOCs emissions. In this scenario, the aerosol nature (secondary organic aerosol from anthropogenic and biogenic precursors) and the predominant regional-scale atmospheric dynamics and circulation appeared to influence the shrinkage event occurrence.

The inter-annual differences found in the shrinkage observations seemed connected to the temperature and precipitation variations relative to the normal climatological situation in the experimental area. This relationship suggests that these meteorological aspects, which condition the temporal variations of BVOCs and the

atmospheric nucleation processes, indirectly influence the development of shrinkages events.

The results of the proposed classification have shown that pure S events were the most represented group for the whole period of study, 30 cases, followed closely by NPF+S events, 28 cases, while 12 cases corresponded to the G+S group. The shrinkage phase was longer in duration for S events (~4 h) than for the NPF+S (~3 h) and G+S events (~3 h). GR and SR varied from 1.4 to 10.6 $nm \cdot h^{-1}$ and -1.0 to -11.1 $nm \cdot h^{-1}$ respectively.

Shrinkages typically appeared in the afternoon, about 18:00 UTC. 67% of the observations were identified under a wind speed exceeding 5 $m \cdot s^{-1}$, in some cases up to 3 times higher than the wind speed recorded in the preceding hours to the shrinkages phase. Also, a reduction in photochemical transformations observed at the end of the day, when the shrinkages occurred, seemed to have a significant contribution to the development of these processes.

As a result of the shrinkage, changes in the particle concentration distributed among the modal size ranges were observed. A shift to smaller particles corresponded to an increase in N_{nuc} and a decrease in N_{Ait}. In some cases, these variations were not as evident and only affected N_{Ait}. In addition, the dilution effect led to a significant reduction in particle concentration during the shrinkage phase of some events, which exceeded 30% for some of them.

Summarizing, the results obtained at this experimental site indicate that the determining factors for the significant number of nucleation-shrinkages identified are two: i) the aerosol nature in the study area, with an important volatile fraction, and ii) the atmospheric dynamics features of the Madrid region. This suggests that, the most likely these events will not take place locally but throughout this region.

In agreement with the available literature on atmospheric aerosol shrinkage events, Ambient conditions and typical characteristics of the measurement area (climate, atmospheric dynamics, emissions, land use…), seem to influence and favor the shrinkage occurrence. However, further research is needed to understand exactly what role play the chemistry and the participating gaseous specie in these processes, aspects still unknown.

Acknowledgments

This work has been partially supported by the Spanish National Research Plan through the project PROACLIM (CGL2014-52877-R) and by the Madrid Regional Research Plan through TECNAIRE (P2013/MAE-2972). The authors wish to thank NOAA Air Resources Laboratory (ARL) for the provision of the HYSPLIT transport and dispersion model and/or READY website (http://www.ready.noaa.gov) used in this publication. Likewise, thanks are also given to José Luis Mosquera for his help in the processing of data which are the core of this work, and Iván Alonso for his help in preparing some of the figures included in this paper.

References

Alonso-Blanco, E., Gómez-Moreno, F. J., Sjogren, S., and Artíñano, B.: Building and tuning-up of an HTDMA and its first measurements in an urban background area, 2nd Iberian Meeting on Aerosol Science and Technology, 2014, 33-38,

Artíñano, B., Pujadas, M., Plaza, J., Crespí, S. N., Cabal, H., Aceña, B., and Terés, J.: Air pollution episodes in the Madrid airshed, in: Transport and Transformation of Pollutants in the Troposphere, SPB Academic Publishing Copenhagen, 294-297, 1994.

Artíñano, B., Salvador, P., Alonso, D. G., Querol, X., and Alastuey, A.: Anthropogenic and natural influence on the PM 10 and PM 2.5 aerosol in Madrid (Spain). Analysis of high concentration episodes, Environmental pollution, 125, 453-465, 2003.

Backman, J., Rizzo, L. V., Hakala, J., Nieminen, T., Manninen, H. E., Morais, F., Aalto, P. P., Siivola, E., Carbone, S., and Hillamo, R.: On the diurnal cycle of urban aerosols, black carbon and the occurrence of new particle formation events in springtime São Paulo, Brazil, Atmospheric Chemistry and Physics, 12, 11733-11751, 2012.

Bianchi, F., Tröstl, J., Junninen, H., Frege, C., Henne, S., Hoyle, C., Molteni, U., Herrmann, E., Adamov, A., and Bukowiecki, N.: New particle formation in the free troposphere: A question of chemistry and timing, Science, 352, 1109-1112, 2016.

Cusack, M., Alastuey, A., and Querol, X.: Case studies of new particle formation and evaporation processes in the western Mediterranean regional background, Atmospheric Environment, 81, 651-659, 2013.

Charlson, R. J.: Atmospheric visibility related to aerosol mass concentration: review, Environmental Science & Technology, 3, 913-918, 1969.

Dal Maso, M., Kulmala, M., Riipinen, I., Wagner, R., Hussein, T., Aalto, P. P., and Lehtinen, K. E. J.: Formation and growth of fresh atmospheric aerosols: eight years of aerosol size distribution data from SMEAR II, Hyytiala, Finland, Boreal Environment Research, 10, 323, 2005.

Donaldson, K., Stone, V., Clouter, A., Renwick, L., and MacNee, W.: Ultrafine particles, Occupational and environmental medicine, 58, 211-216, 2001.

Ehn, M., Kleist, E., Junninen, H., Petäjä, T., Lönn, G., Schobesberger, S., Maso, M. D., Trimborn, A., Kulmala, M., and Worsnop, D.: Gas phase formation of extremely oxidized pinene reaction products in chamber and ambient air, Atmospheric chemistry and physics, 12, 5113-5127, 2012.

Ehn, M., Thornton, J. A., Kleist, E., Sipilä, M., Junninen, H., Pullinen, I., Springer, M., Rubach, F., Tillmann, R., and Lee, B.: A large source of low-volatility secondary organic aerosol, Nature, 506, 476-479, 2014.

Gómez-Moreno, F., Alonso-Blanco, E., Artíñano, B., Juncal-Bello, V., Iglesias-Samitier, S., Piñeiro Iglesias, M., López Mahía, P., Perez, N., Pey, J., Ripoll, A., Alastuey, A., de la Morena, B., García, M.,

Rodríguez, S., Sorribas, M., Titos, G., Lyamani, H., Lucas, A.-A., Latorre, E., Tritscher, T., and Bischof, O.: Intercomparisons of mobility size spectrometers and condensation particle counters in the frame of the Spanish atmospheric observational aerosol network, Aerosol Science & Technology, accepted, 2015.

Gómez-Moreno, F. J., Artíñano, B., Piñeiro Iglesias, M., López Mahía, P., Pey, J., Alastuey, A., Sorribas, M., de la Morena, B. A., and Rodríguez, S.: The Spanish Network on Environmental DMAs: Introduction and main activities, IV Spanish Meeting on Aerosol Science and Technology – RECTA 2010, 28-30 June, Granada, Spain. ISBN: 978-84-693-4839-0. , 2010.

Gómez-Moreno, F. J., Pujadas, M., Plaza, J., Rodríguez-Maroto, J. J., Martínez-Lozano, P., and Artiñano, B.: Influence of seasonal factors on the atmospheric particle number concentration and size distribution in Madrid, Atmospheric Environment, 45, 3169-3180, 2011.

Gómez-Moreno, F. J., Alonso, E., Artíñano, B., Rodríguez-Maroto, J., Rojas, E., Piñeiro Iglesias, M., López Mahía, P., Pérez, N., Alastuey, A., Archilla, V., Titos, G., Alados-Arboledas, L., Borrás, E., Muñoz, A., Tritscher, T., Filimundi, E., and Latorre, E.: An Intercomparison Campaign for CPC, SMPS and UFPM in the Frame of the REDMAAS Network, IV Iberian Meeting on Aerosol Science and Technology – RICTA 2016, 29 June-01 July, Aveiro, Portugal. Proceedings Book., 2016.

Hamed, A., Korhonen, H., Sihto, S.-L., Joutsensaari, J., Järvinen, H., Petäjä, T., Arnold, F., Nieminen, T., Kulmala, M., and Smith, J. N.: The role of relative humidity in continental new particle formation, Journal of Geophysical Research: Atmospheres (1984-2012), 116, 2011.

Harrison, R. M., and Yin, J.: Particulate matter in the atmosphere: which particle properties are important for its effects on health?, Science of the total environment, 249, 85-101, 2000.

IPCC: Climate Change 2013: The Physical Science Basis., 2013.

Kecorius, S., Zhang, S., Wang, Z., Größ, J., Ma, N., Wu, Z., Ran, L., Hu, M., Wang, P., and Ulevičius, V.: Nocturnal aerosol particle formation in the North China Plain, Lithuanian Journal of Physics, 55, 2015.

Kim, Y., Kim, S.-W., Yoon, S.-C., Park, J.-S., Lim, J.-H., Hong, J., Lim, H.-C., Ryu, J., Lee, C.-K., and Heo, B.-H.: Characteristics of formation and growth of atmospheric nanoparticles observed at four regional background sites in Korea, Atmospheric Research, 168, 80-91, 2016.

Kirkby, J., Duplissy, J., Sengupta, K., Frege, C., Gordon, H., Williamson, C., Heinritzi, M., Simon, M., Yan, C., and Almeida, J.: Ion-induced nucleation of pure biogenic particles, Nature, 533, 521-526, 2016.

Kontkanen, J., Lehtipalo, K., Ahonen, L., Kangasluoma, J., Manninen, H. E., Hakala, J., Rose, C., Sellegri, K., Xiao, S., and Wang, L.: Measurements of sub-3 nm particles using a particle size magnifier in different environments: from clean mountain top to polluted megacities, Atmospheric Chemistry and Physics, 17, 2163-2187, 2017.

Kulmala, M., and Laaksonen, A.: Binary nucleation of water-sulfuric acid system: Comparison of classical theories with different H_2SO_4 saturation vapor pressures, The Journal of Chemical Physics, 93, 696-701, 1990.

Kulmala, M., Pirjola, L., and Mäkelä, J. M.: Stable sulphate clusters as a source of new atmospheric particles, Nature, 404, 66-69, 2000.

Kulmala, M., Petäjä, T., Nieminen, T., Sipilä, M., Manninen, H. E., Lehtipalo, K., Dal Maso, M., Aalto, P. P., Junninen, H., and Paasonen, P.: Measurement of the nucleation of atmospheric aerosol particles, Nature protocols, 7, 1651-1667, 2012.

Kulmala, M., Petäjä, T., Ehn, M., Thornton, J., Sipilä, M., Worsnop, D., and Kerminen, V.-M.: Chemistry of atmospheric nucleation: on the recent advances on precursor characterization and atmospheric cluster composition in connection with atmospheric new particle formation, Annual review of physical chemistry, 65, 21-37, 2014.

Kusaka, I., Wang, Z. G., and Seinfeld, J. H.: Binary nucleation of sulfuric acid-water: Monte Carlo simulation, The Journal of chemical physics, 108, 6829-6848, 1998.

Lehtinen, K. E. J., Korhonen, H., Maso, M. D., and Kulmala, M.: On the concept of condensation sink diameter, Boreal Environment Research, 8, 405-412, 2003.

Lihavainen, H., Alghamdi, M., Hyvärinen, A.-P., Hussein, T., Aaltonen, V., Abdelmaksoud, A., Al-Jeelani, H., Almazroui, M., Almehmadi, F., and Al Zawad, F.: Aerosols physical properties at Hada Al Sham, western Saudi Arabia, Atmospheric Environment, 135, 109-117, 2016.

Lyman, W. J., Reehl, W. F., and Rosenblatt, D. H.: Handbook of chemical property estimation methods: environmental behavior of organic compounds, 1990.

Mikkonen, S., Romakkaniemi, S., Smith, J. N., Korhonen, H., Petäjä, T., Plass-Duelmer, C., Boy, M., McMurry, P. H., Lehtinen, K. E. J., and Joutsensaari, J.: A statistical proxy for sulphuric acid concentration, Atmospheric Chemistry and Physics, 11, 11319-11334, 2011.

Neitola, K., Hyvärinen, A., Lihavainen, H., Alghamdi, M., Hussein, T., Khodeir, M., Shehata, A., Laaksonen, A., and Kulmala, M.: New Particle Formation Events During 2013 in Hada Al Sham, Saudi-Arabia, AGU Fall Meeting Abstracts, 2014, 3131,

Oberdörster, G., Oberdörster, E., and Oberdörster, J.: Nanotoxicology: an emerging discipline evolving from studies of ultrafine particles, Environmental health perspectives, 823-839, 2005.

Pirjola, L., Kulmala, M., Wilck, M., Bischoff, A., Stratmann, F., and Otto, E.: Formation of Sulphuric Acid Aerosols and Cloud Condensation Nuclei: An Expression for Significant Nucleation and Model Comprarison, Journal of Aerosol Science, 30, 1079-1094, 1999.

Platt, U., and Stutz, J.: Differential optical absorption spectroscopy. Principles and applications, Springer Berlin Heidelberg, 2008.

Plaza, J., and Artíñano, B.: Characterization of pollutants cycles evolution in a coastal mediterranean area under summer conditions, Centro de Investigaciones Energeticas Medioambientales y Tecnologicas (CIEMAT), Madrid (Spain), 1994.

Pujadas, M., Plaza, J., Terés, J., Artíñano, B., and Millán, M.: Passive remote sensing of nitrogen dioxide as a tool for tracking air pollution in urban areas: the Madrid urban plume, a case of study, Atmospheric Environment, 34, 3041-3056, 2000.

Robinson, A. L., Donahue, N. M., Shrivastava, M. K., Weitkamp, E. A., Sage, A. M., Grieshop, A. P., Lane, T. E., Pierce, J. R., and Pandis, S. N.: Rethinking organic aerosols: semivolatile emissions and photochemical aging, Science, 315, 1259-1262, 10.1126/science.1133061, 2007.

Rolph, G.: Real-time Environmental Applications and Display sYstem (READY) Website (http://ready. arl. noaa. gov). NOAA Air Resources Laboratory, Silver Spring, Silver Spring, MD, 2016.

Salma, I., Németh, Z., Kerminen, V.-M., Aalto, P., Nieminen, T., Weidinger, T., Molnár, Á., Imre, K., and Kulmala, M.: Regional effect on urban atmospheric nucleation, Atmospheric Chemistry and Physics, 16, 8715-8728, 2016a.

Salma, I., Németh, Z., Weidinger, T., Kovács, B., and Kristóf, G.: Measurement, growth types and shrinkage of newly formed aerosol particles at an urban research platform, Atmos. Chem. Phys, 16, 7837-7851, 2016b.

Salvador, P.: Characterization of air pollution produced by particles in suspension in Madrid., Doctoral Thesis. Faculty of Physics, University Complutense of Madrid, Madrid (Spain). 2004.

Salvador, P., Artíñano, B., Alonso, D. G., Querol, X., and Alastuey, A.: Identification and characterisation of sources of PM10 in Madrid (Spain) by statistical methods, Atmospheric Environment, 38, 435-447, 2004.

Salvador, P., Artíñano, B., Viana, M., Alastuey, A., and Querol, X.: Evaluation of the changes in the Madrid metropolitan area influencing air quality: Analysis of 1999-2008 temporal trend of particulate matter, Atmospheric Environment, 57, 175-185, 2012.

Seinfeld, J. H., and Pandis, S. N.: Atmospheric chemistry and physics: from air pollution to climate change, John Wiley & Sons, 2016.

Siakavaras, D., Samara, C., Petrakakis, M., and Biskos, G.: Nucleation events at a coastal city during the warm period: Kerbside versus urban background measurements, Atmospheric Environment, 140, 60-68, 2016.

Skrabalova, L., Zikova, N., and Zdimal, V.: Shrinkage of Newly Formed Particles in an Urban Environment, Aerosol and Air Quality Research, (Article in press), 2015.

Stein, A., Draxler, R., Rolph, G., Stunder, B., Cohen, M., and Ngan, F.: NOAA's HYSPLIT atmospheric transport and dispersion modeling system, Bulletin of the American Meteorological Society, 96, 2059-2077, 2015.

713 Tröstl, J., Chuang, W. K., Gordon, H., Heinritzi, M., Yan, C., Molteni, U., Ahlm, L., Frege, C., Bianchi,
714 F., and Wagner, R.: The role of low-volatility organic compounds in initial particle growth in the
715 atmosphere, Nature, 533, 527-531, 2016.

716 Vehkamäki, H., Maso, M. D., Hussein, T., Flanagan, R., Hyvärinen, A., Lauros, J., Merikanto, P.,
717 Mönkkönen, M., Pihlatie, K., and Salminen, K.: Atmospheric particle formation events at Värriö
718 measurement station in Finnish Lapland 1998-2002, Atmospheric Chemistry and Physics, 4, 2015-2023,
719 2004.

720 Vogel, A. L., Schneider, J., Müller-Tautges, C., Klimach, T., and Hoffmann, T.: Aerosol Chemistry
721 Resolved by Mass Spectrometry: Insights into Particle Growth after Ambient New Particle Formation,
722 Environmental Science & Technology, 50, 10814-10822, 2016.

723 Watson, J. G.: Visibility: Science and regulation, Journal of the Air & Waste Management Association, 52,
724 628-713, 2002.

725 Wiedensohler, A., Birmili, W., Nowak, A., Sonntag, A., Weinhold, K., Merkel, M., Wehner, B., Tuch, T.,
726 Pfeifer, S., and Fiebig, M.: Mobility particle size spectrometers: harmonization of technical standards and
727 data structure to facilitate high quality long-term observations of atmospheric particle number size
728 distributions, Atmospheric Measurement Techniques, 5, 657-685, 2012.

729 Xiao, S., Wang, M., Yao, L., Kulmala, M., Zhou, B., Yang, X., Chen, J., Wang, D., Fu, Q., and Worsnop,
730 D.: Strong atmospheric new particle formation in winter in urban Shanghai, China, Atmospheric Chemistry
731 and Physics, 15, 1769-1781, 2015.

732 Yao, X., Choi, M. Y., Lau, N. T., Lau, A. P. S., Chan, C. K., and Fang, M.: Growth and shrinkage of new
733 particles in the atmosphere in Hong Kong, Aerosol Science and Technology, 44, 639-650, 2010.

734 Young, L.-H., Lee, S.-H., Kanawade, V., Hsiao, T.-C., Hwang, B.-F., Liou, Y.-J., Hsu, H.-T., and Tsai, P.-
735 J.: New particle growth and shrinkage observed in subtropical environments, Atmospheric Chemistry and
736 Physics, 13, 547-564, 2013.

737 Yu, H., Zhou, L., Dai, L., Shen, W., Dai, W., Zheng, J., Ma, Y., and Chen, M.: Nucleation and growth of
738 sub-3 nm particles in the polluted urban atmosphere of a megacity in China, Atmospheric Chemistry and
739 Physics, 16, 2641-2657, 2016.

740

741 **Figures**

742 Fig. 1 (A) CIEMAT facilities and their surrounding environments and (B) location of the
743 sampling point.

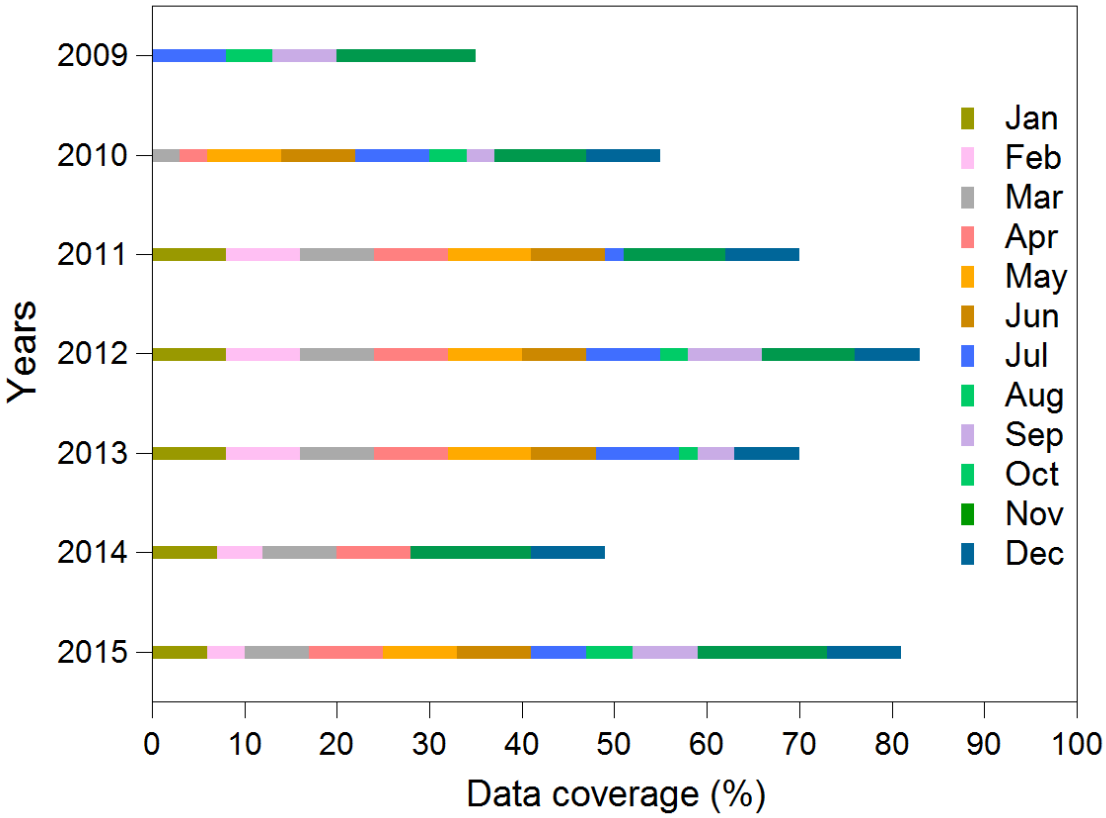

744 Fig. 2 2009–2015 data coverage obtained from the SMPS.

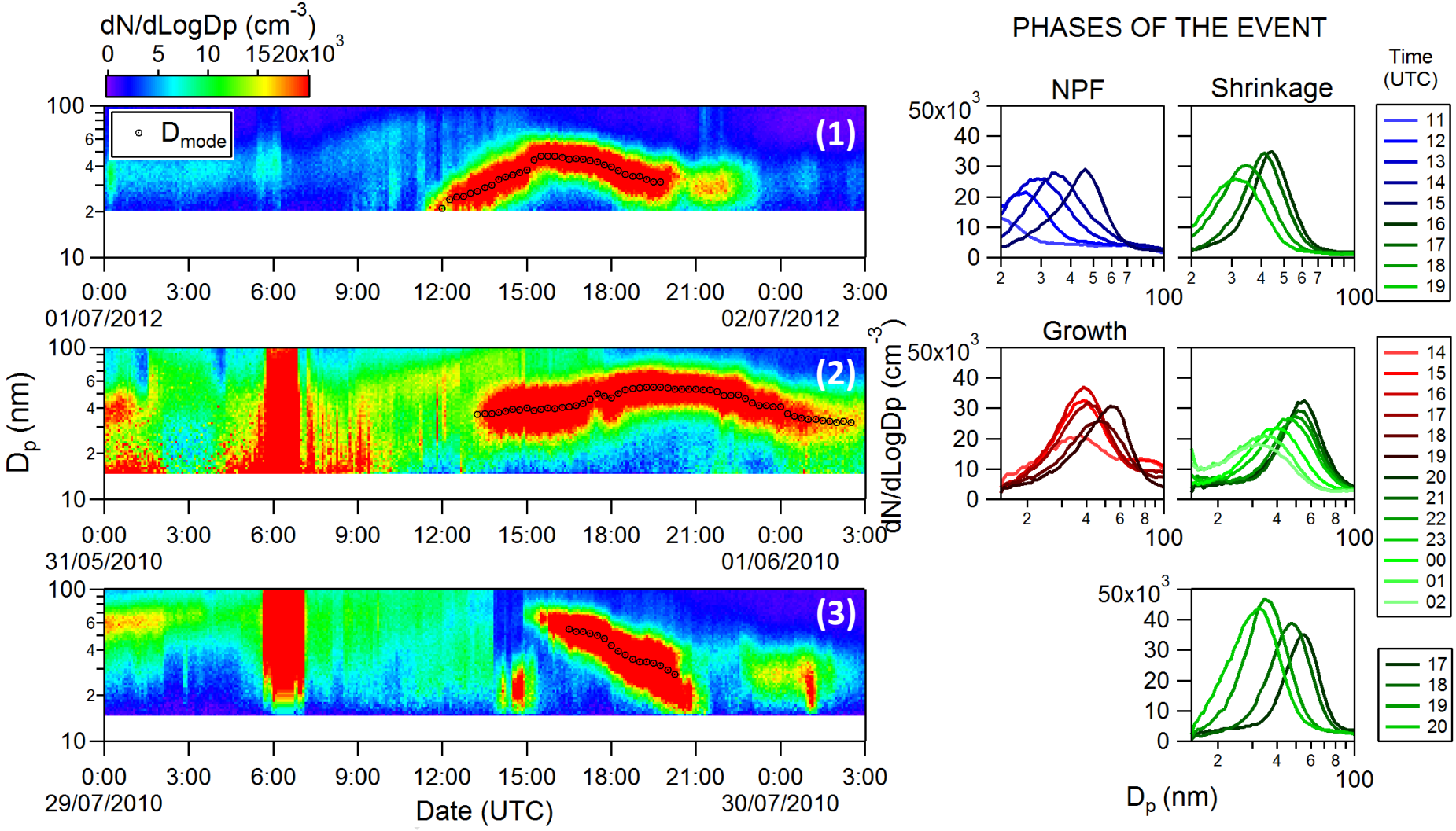
dN/dLogDp (cm-3)
0 5 10 15 20x10^3
D_mode
(1)
(2)
(3)
D_p (nm)
100
6
4
2
10
0:00 3:00 6:00 9:00 12:00 15:00 18:00 21:00 0:00 3:00
01/07/2012
02/07/2012
31/05/2010
01/06/2010
29/07/2010
30/07/2010
Date (UTC)
dN/dLogDp (cm-3)
PHASES OF THE EVENT
NPF
Shrinkage
Growth
Time (UTC)
50x10^3
40
30
20
10
0
2 3 4 5 6 7
100
11 12 13 14 15 16 17 18 19
14 15 16 17 18 19 20 21 22 23 00 01 02
17 18 19 20
D_p (nm)

745 Fig. 3 Proposed classification for the study of aerosol particle shrinkage events: example of each group of shrinkages ((1) NPF+shrinkage (NPF+S)
746 events, (2) aerosol particle growth process+shrinkage (G+S) events and (3) pure shrinkage (S) events), showing hourly time evolution of particle
747 size distribution during each phase (NPF, growth and shrinkage phases).

748

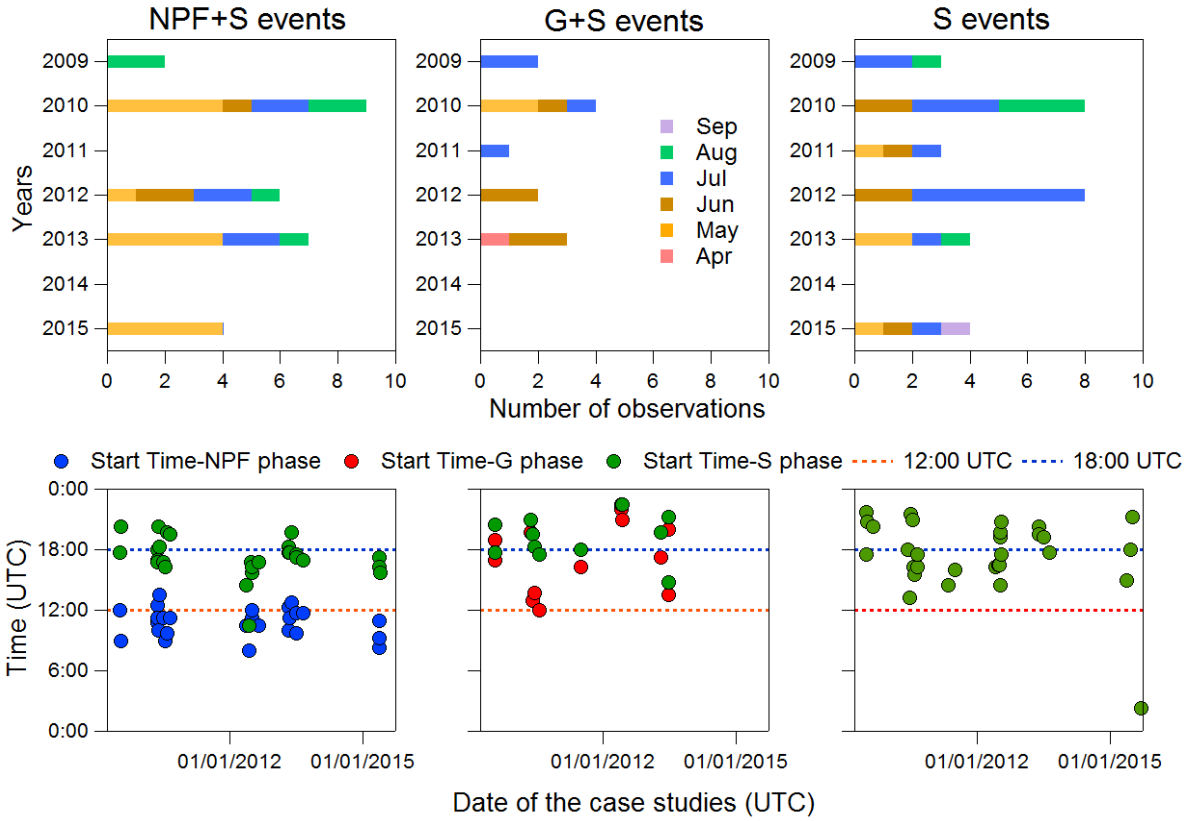

749 Fig. 4 Number of observations per month for each group of categorized event at the CIEMAT site during 2009–2015, as well as the starting time
750 of each phase of the event (NPF, growth and shrinkage phases). The orange dotted line corresponds to midday (12:00 UTC) and the blue dotted
751 line to mid-afternoon (18:00 UTC).

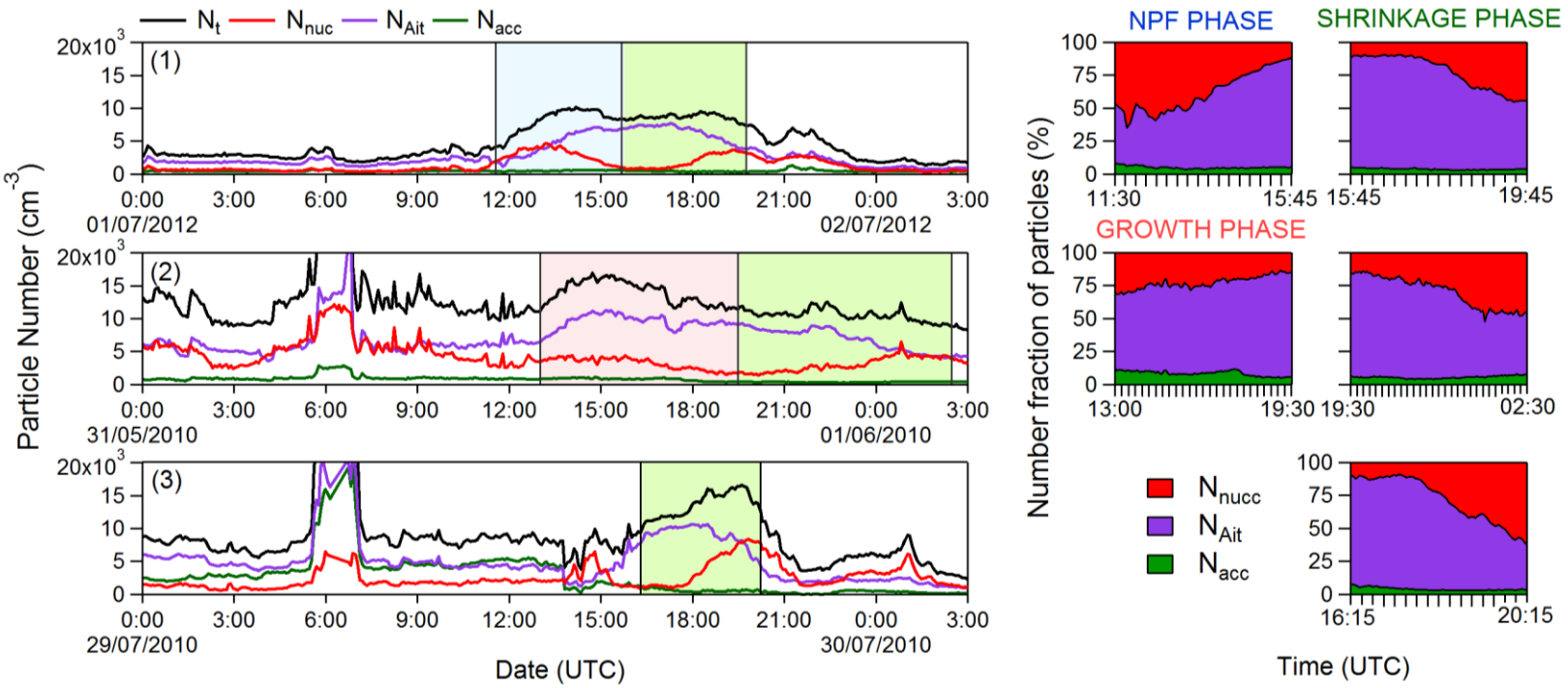

752 Fig. 5 Typical example of the evolution of the total (N_t) and modal particle concentration (N_{nuc}, N_{Ait}, and N_{acc}) for each group of shrinkages ((1)
753 NPF+shrinkage (NPF+S) events, (2) growth process+shrinkage (G+S) events and (3) pure shrinkage (S) events), representing the progress of the
754 modal numerical fraction for each phase of the events for 15 minutes average time intervals. The shaded area in the graph represents each phase
755 of the event (blue shaded zone=NPF phase, red shaded zone=aerosol particle growth phase and green shaded zone=shrinkage phase).

756

Tables

Table 1 Summary of shrinkages processes studies of atmospheric particles.

Reference paper	Site class	Climate	Study period	Period when the shrinkages were identified	Shrinkage Event Group	Num. of Observations	Shrinkage time start (in Local Time (LT) or UTC)	Duration of the Shrinkage phase	SR* ($nm \cdot h^{-1}$)	Causes of the shrinkage processes
This study	Urban background	Continental-Mediterranean	Jul. 2009 to Dec.2015 (67 months)	Spring and summer seasons	NPF+S G+S S	28 12 30	~ 18:00 UTC	From 1 to 8.5 h	Between -1.0 and -11.1	Increase in wind speed and decrease in photochemical activity
Lihavainen et al. (2016)	Rural background	Arid	Nov. 2012 to Feb. 2015 (data coverage of 64%)	-	NPF+S	-	In the afternoon	-	-	-
Salma et al. (2016)	Urban	Humid continental	3 years	Spring and summer seasons	NPF+S	8	~ 12:00 UTC	From 1.5 to 2 h.		Increase in wind speed and decrease in photochemical
Skrabalova et al. (2015)	Urban background	Continental	May 2012 to Apr. 2014 (24 months)	Spring and summer seasons and exceptionally autumn season	NPF+S	22	~ 12:00 UTC	> 2 h	Between -2.5 and -12.5	Increase in wind speed, high ambient temperature and decrease in photochemical activity

Cusack et al. (2013)	Regional background	Mediterranean	Oct. 2010 to Jun. 2011 (9 months)	Spring season	NPF+S S Not defined in the paper	1 1 5	Between 12:30 and 15:30 UTC	From 1 to 4 h	Between 3.1 and 11.1	High ambient temperature
Young et al. (2013)	Coastal, urban, and downwind	Subtropical	Oct. 2008 to Jan.2009 and Aug. 2010 to Oct.2010 (7 months)	Warm season	NPF+S	5	Between 11:09 and 13:26 LT	-	Between -5.1 and -7.6	Increase in wind speed and high ambient temperature
Backman et al. (2012)	Urban background	Subtropical	10 Oct. 2010 to 10 Jun. 2011 (9 months)	-	S	1	14:00 LT	-	5.2	High ambient temperature
Yao et al. (2010)	Coastal suburban	Subtropical	Feb. 2003 to Jan. 2004 (12 months)	-	NPF+S	2	12:30 and 15:00 UTC	-	8.6 and 10.7	Increase in wind speed and decrease in photochemical activity

*SR can be a positive or a negative value depending on the methodology used by each author.

761 Table 2. Time distribution of the shrinkage events during 2009-2015 and the availability of SMPS data (in %) when they occurred. Data during
762 the warm period of 2014 are not available owing to a temporary instrument failure of the SMPS system.

Month	2009		2010		2011		2012		2013		2014		2015	
	Num. of cases	Data coverage	Num. of cases	Data coverage	Num. of cases	Data coverage	Num. of cases	Data coverage	Num. of cases	Data coverage	Num. of cases	Data coverage	Num. of cases	Data coverage
Apr.		-		40		100		99	1	98		99		91
May		-	6	99	1	99	1	88	6	98		7	5	99
Jun.		-	4	90	1	99	6	88	2	93		-	1	98
July	6	92	6	96	2	24	8	96	3	99		-	1	75
Aug.	1	58	5	55		-	1	36	2	35		-		62
Sep.		86		39		-		100		37		-	1	73
Total	7	39	21	70	4	54	16	84	14	77		18	8	83

763

Supplementary material

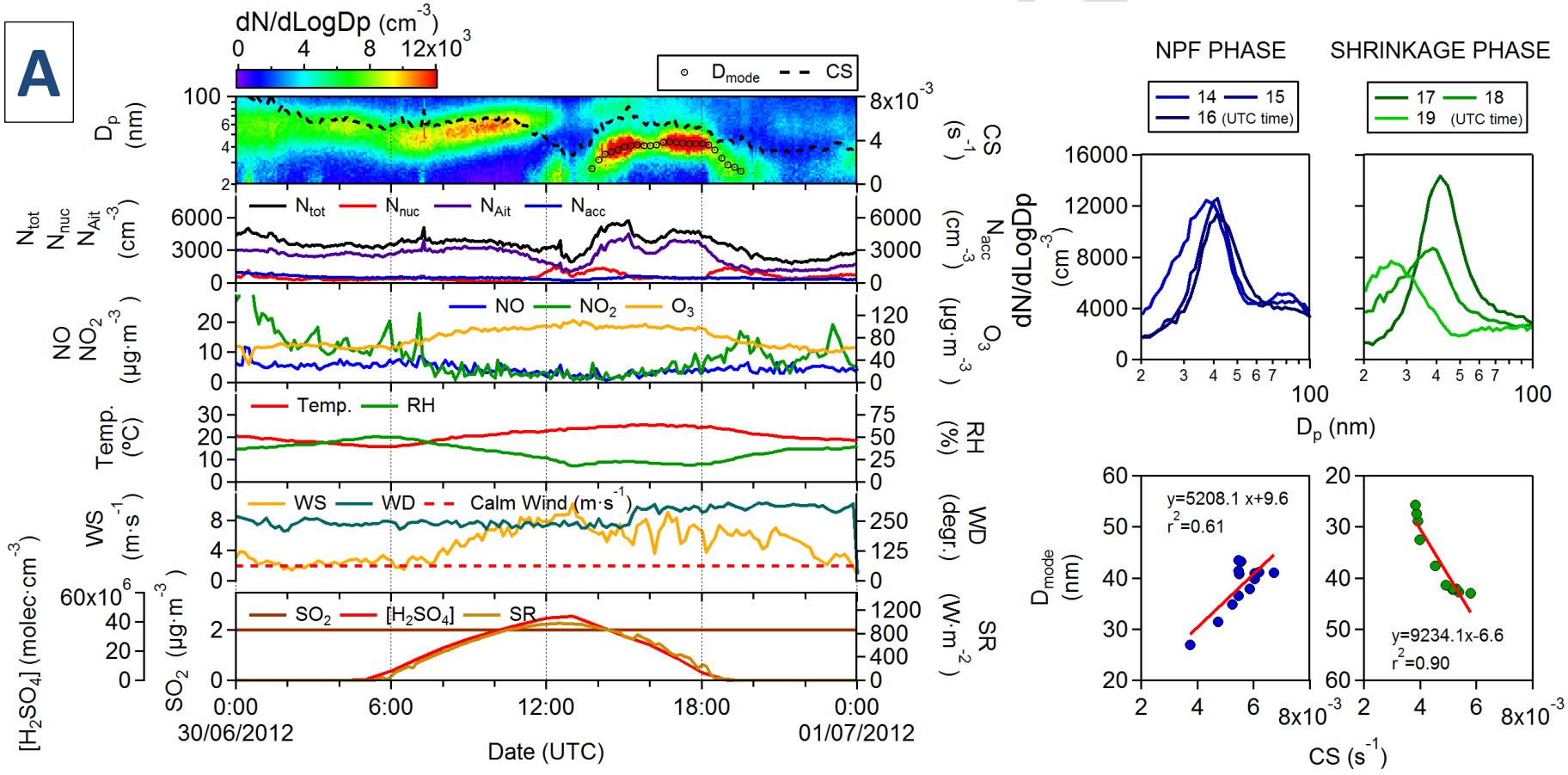

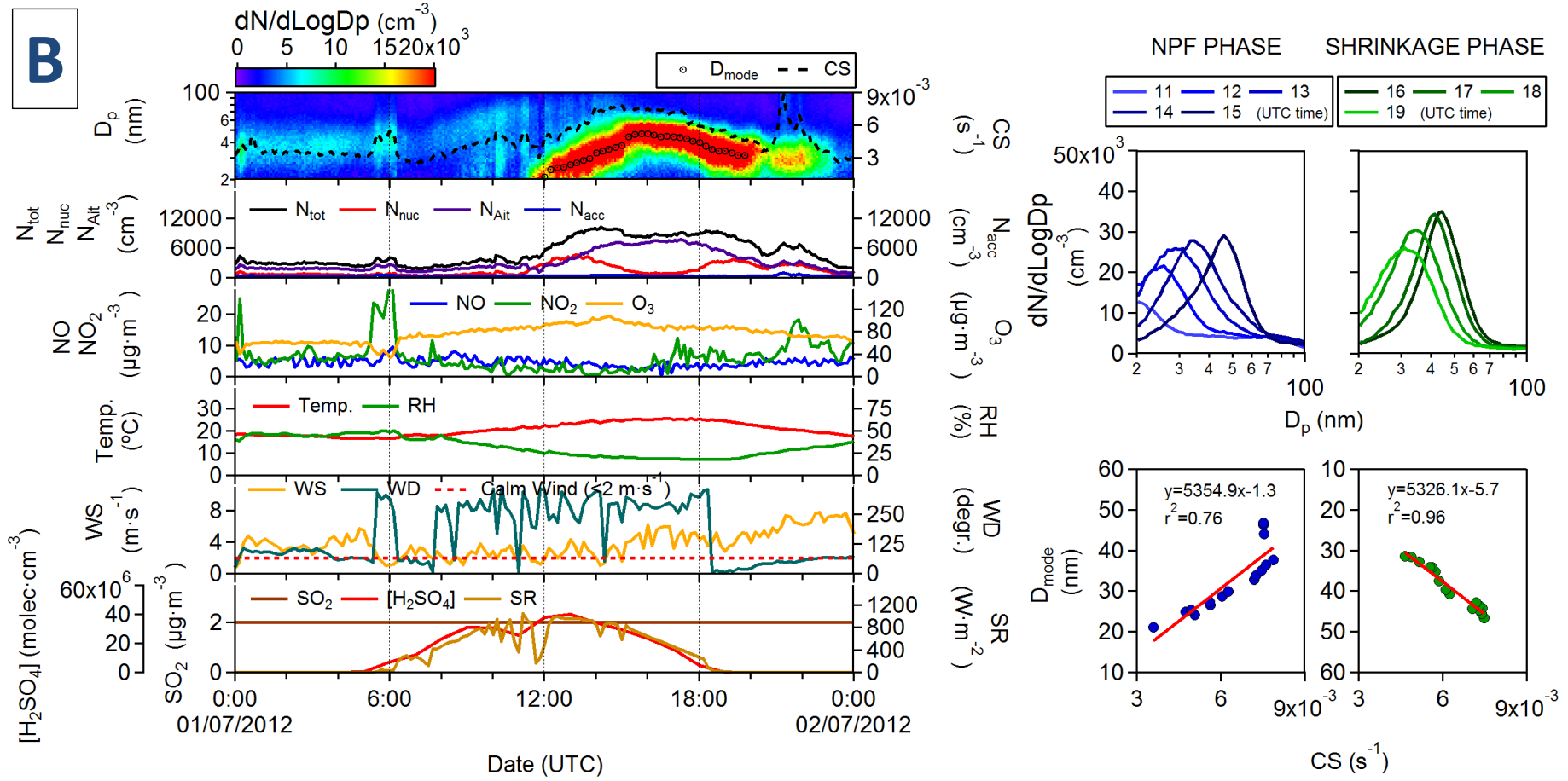

765 Fig. S1 Examples ~~of a~~ of two complete studies ~~for a~~ of two NPF+S events identified on A) 30 June 2012 and B) 1 July 2012. Evolution of the
766 aerosol size distributions and total (N_{tot}) and modal (N_{nuc}, N_{Ait} and N_{acc}) particle number concentrations in relation to air mass composition (SO_2,
767 NO_x and O_3) and meteorological variables (Temp.=Temperature, RH=Relative Humidity, WS=Wind Speed, WD=Wind Direction, SR=Solar

768 Radiation) are represented. D_{mode} estimation, gas-phase H_2SO_4 proxy value and CS have also been included. The gradual shift of 1-h average
769 aerosol size distributions and the correlation between D_{mode} and CS for each phase of the event (NPF and shrinkage phase) is shown on the right
770 side of the graph. Given that the site has a clean background, the time evolution of particle size distributions has been drawn up to 100 nm.

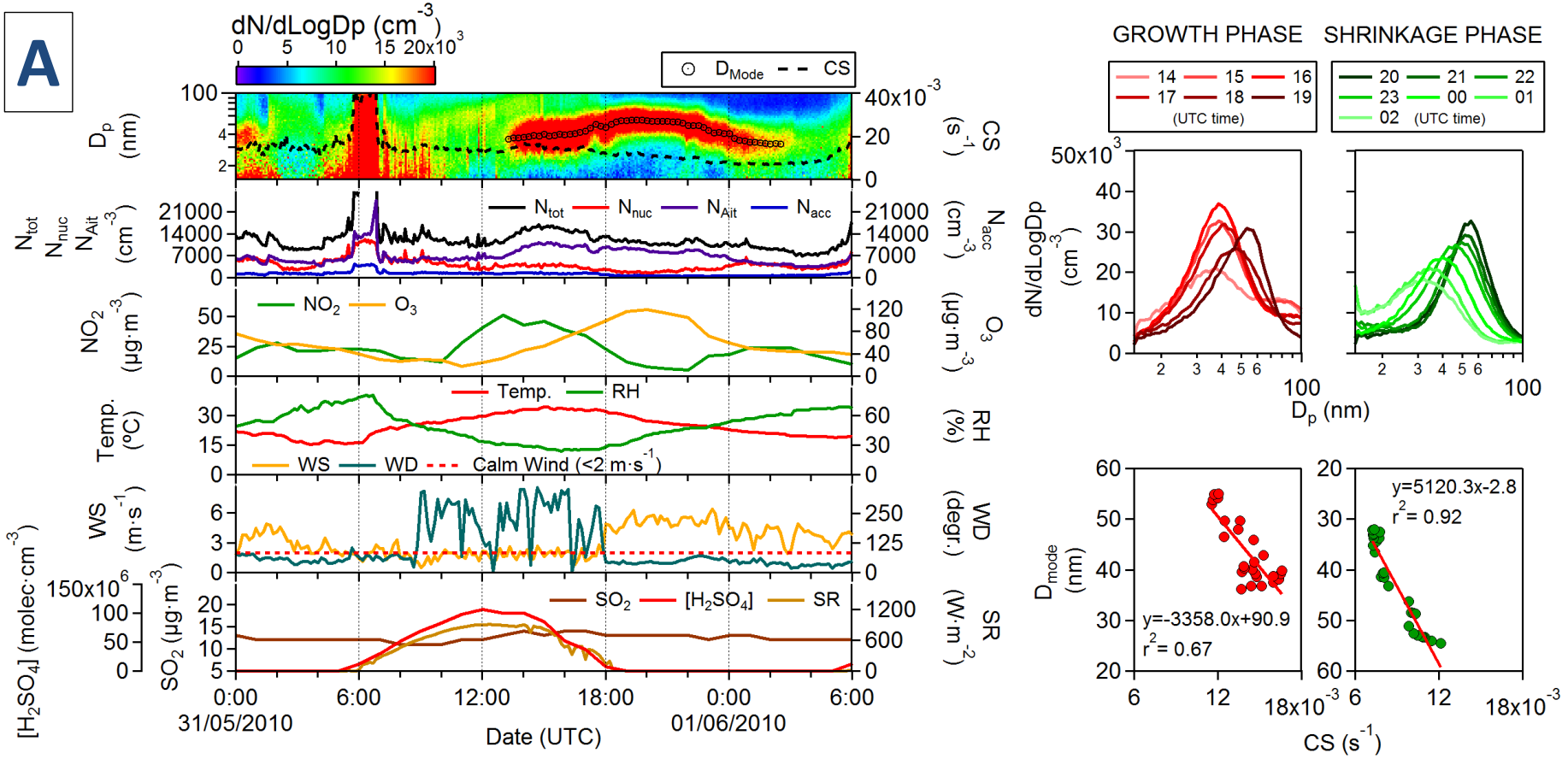
A
dN/dLogDp (cm-3)
0 5 10 15 20x10^3
DMode
CS
Dp (nm)
CS (s-1)
Ntot
Nnuc
NAit
Nacc
(cm-3)
NO2
O3
(µg·m-3)
Temp. (ºC)
RH (%)
WS
WD
WS (m·s-1)
WD (degr.)
Calm Wind (<2 m·s-1)
[H2SO4] (molec·cm-3)
SO2 (µg·m-3)
SR (W·m-2)
0:00
6:00
12:00
18:00
0:00
6:00
31/05/2010
01/06/2010
Date (UTC)
GROWTH PHASE
SHRINKAGE PHASE
14 15 16
17 18 19
(UTC time)
20 21 22
23 00 01
02 (UTC time)
dN/dLogDp (cm-3)
Dp (nm)
Dmode (nm)
y=-3358.0x+90.9
r2= 0.67
y=5120.3x-2.8
r2= 0.92
CS (s-1)

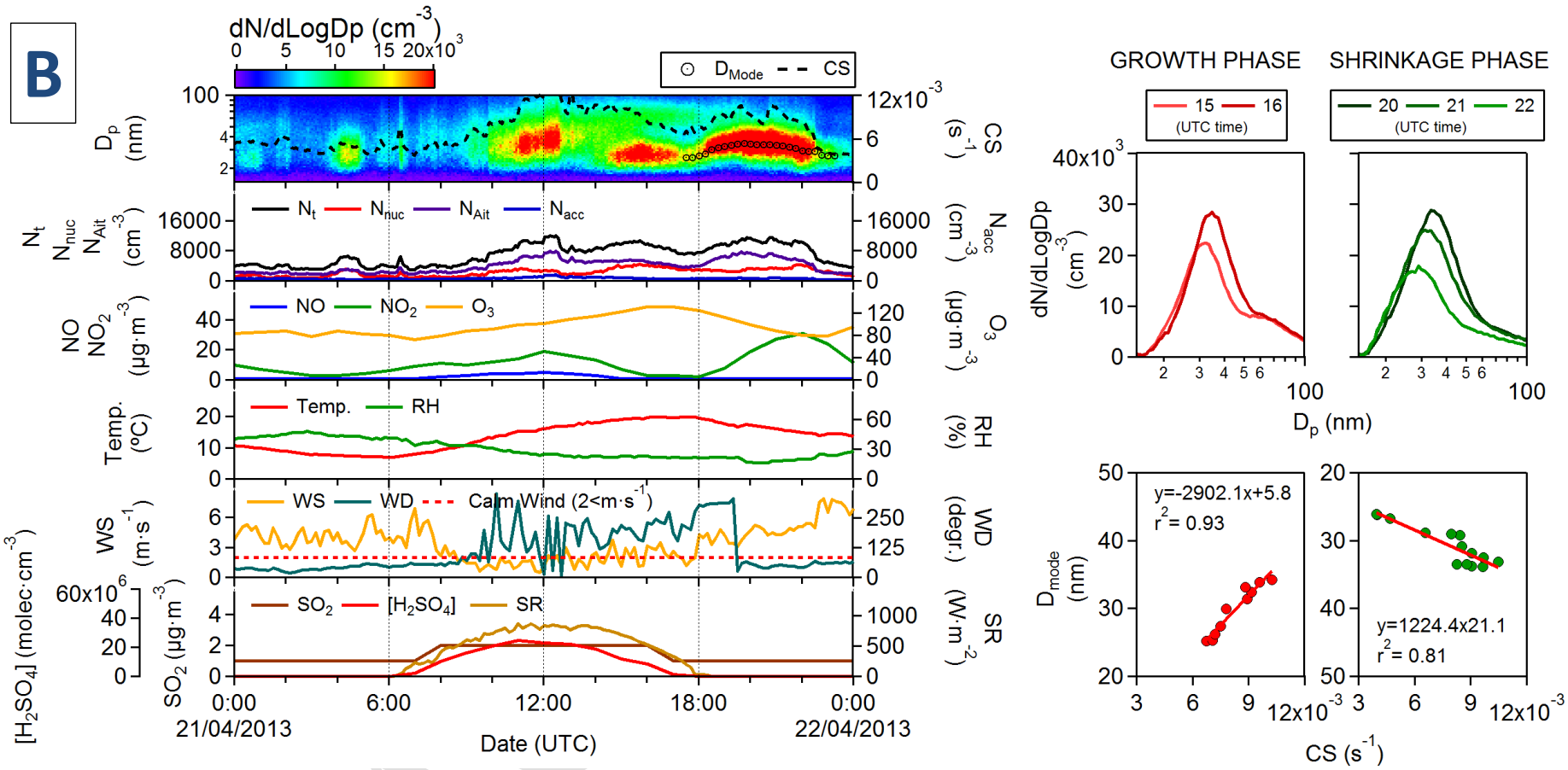
B
dN/dLogDp (cm-3)
0 5 10 15 20x10^3
DMode
CS
Dp (nm)
CS (s-1)
Nt
Nnuc
NAit
Nacc
(cm-3)
NO
NO2
O3
(µg·m-3)
Temp. (ºC)
RH (%)
WS (m·s-1)
WD (degr.)
Calm Wind (2<m·s-1)
SO2 (µg·m-3)
[H2SO4] (molec·cm-3)
SR (W·m-2)
0:00
6:00
12:00
18:00
0:00
21/04/2013
22/04/2013
Date (UTC)
GROWTH PHASE
SHRINKAGE PHASE
15 16
20 21 22
(UTC time)
dN/dLogDp (cm-3)
Dp (nm)
Dmode (nm)
y=-2902.1x+5.8
r2= 0.93
y=1224.4x21.1
r2= 0.81
CS (s-1)

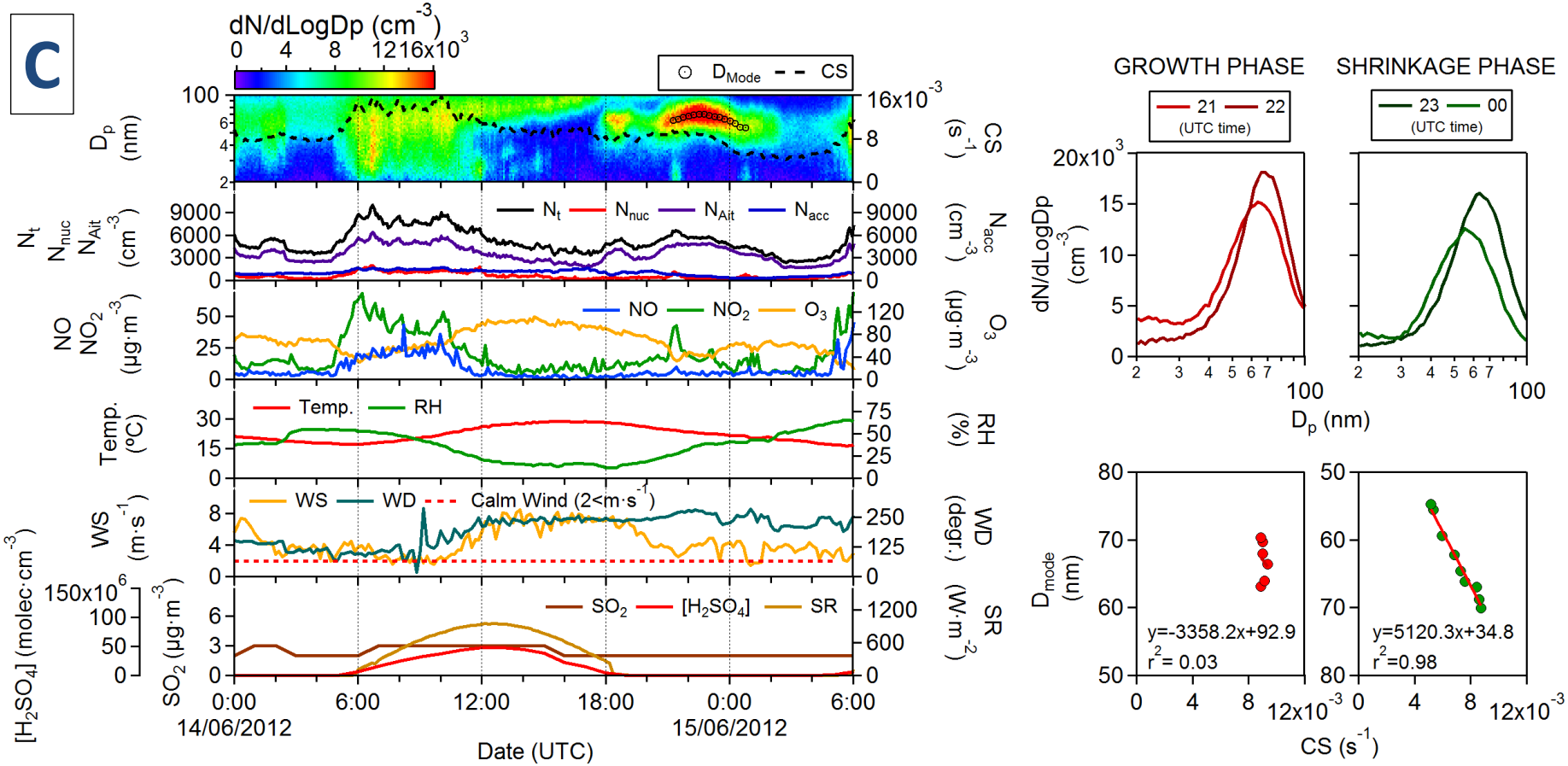

771 Fig. S2 Example of a complete study for each type of G+S event identified on A) 31 May 2010 (G+S event in the morning under a polluted
772 air from traffic), B) 21 March 2013 (G+S event in the afternoon under a polluted air from traffic) and C) 14 June 2012 (G+S event in the afternoon

under an air mass free of traffic emissions). Evolution of the aerosol size distributions and total (N_{tot}) and modal (N_{nuc}, N_{Ait} and N_{acc}) particle number concentrations in relation to air mass composition (SO_2, NO_x and O_3) and meteorological variables (Temp.=Temperature, RH=Relative Humidity, WS=Wind Speed, WD=Wind Direction, SR=Solar Radiation) are represented. D_{mode} estimation, gas-phase H_2SO_4 proxy value and CS have also been included. The gradual shift of 1-h average aerosol size distributions and the correlation between D_{mode} and CS for each phase of the event (aerosol growth and shrinkage phase) is shown on the right side of the graph. Given that the site has a clean background, the time evolution of particle size distributions has been drawn up to 100 nm.

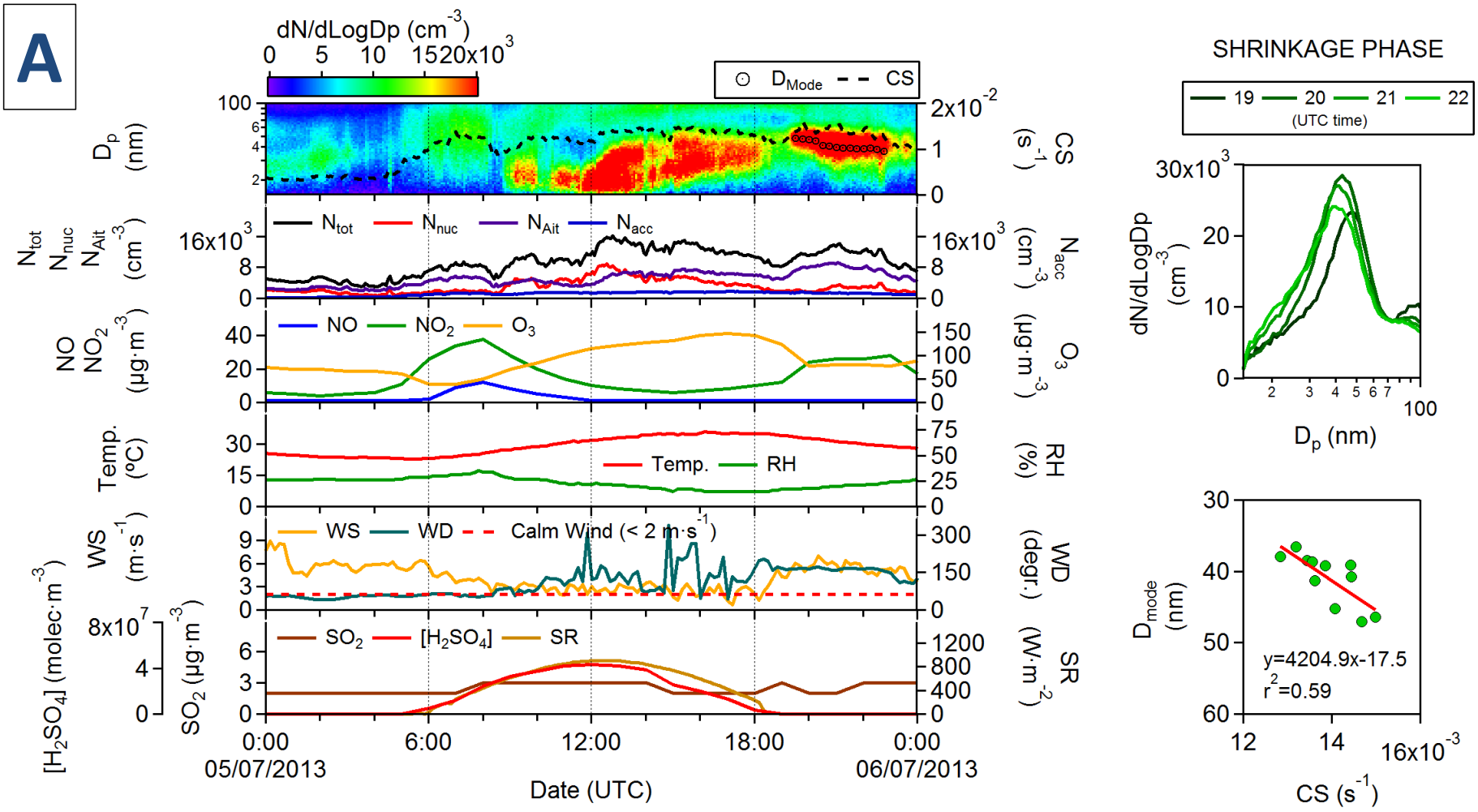
A
dN/dLogDp (cm-3)
0 5 10 1520x10^3
D_Mode
CS
D_p (nm)
CS (s-1)
N_tot
N_nuc
N_Ait
N_acc
(cm-3)
NO
NO2
O3
(µg·m-3)
Temp. (ºC)
RH (%)
WS (m·s-1)
WD (degr.)
Calm Wind (< 2 m·s-1)
[H2SO4] (molec·m-3)
SO2 (µg·m-3)
SR (W·m-2)
0:00
05/07/2013
6:00
12:00
18:00
0:00
06/07/2013
Date (UTC)
SHRINKAGE PHASE
19 20 21 22
(UTC time)
dN/dLogDp (cm-3)
D_p (nm)
D_mode (nm)
y=4204.9x-17.5
r2=0.59
CS (s-1)

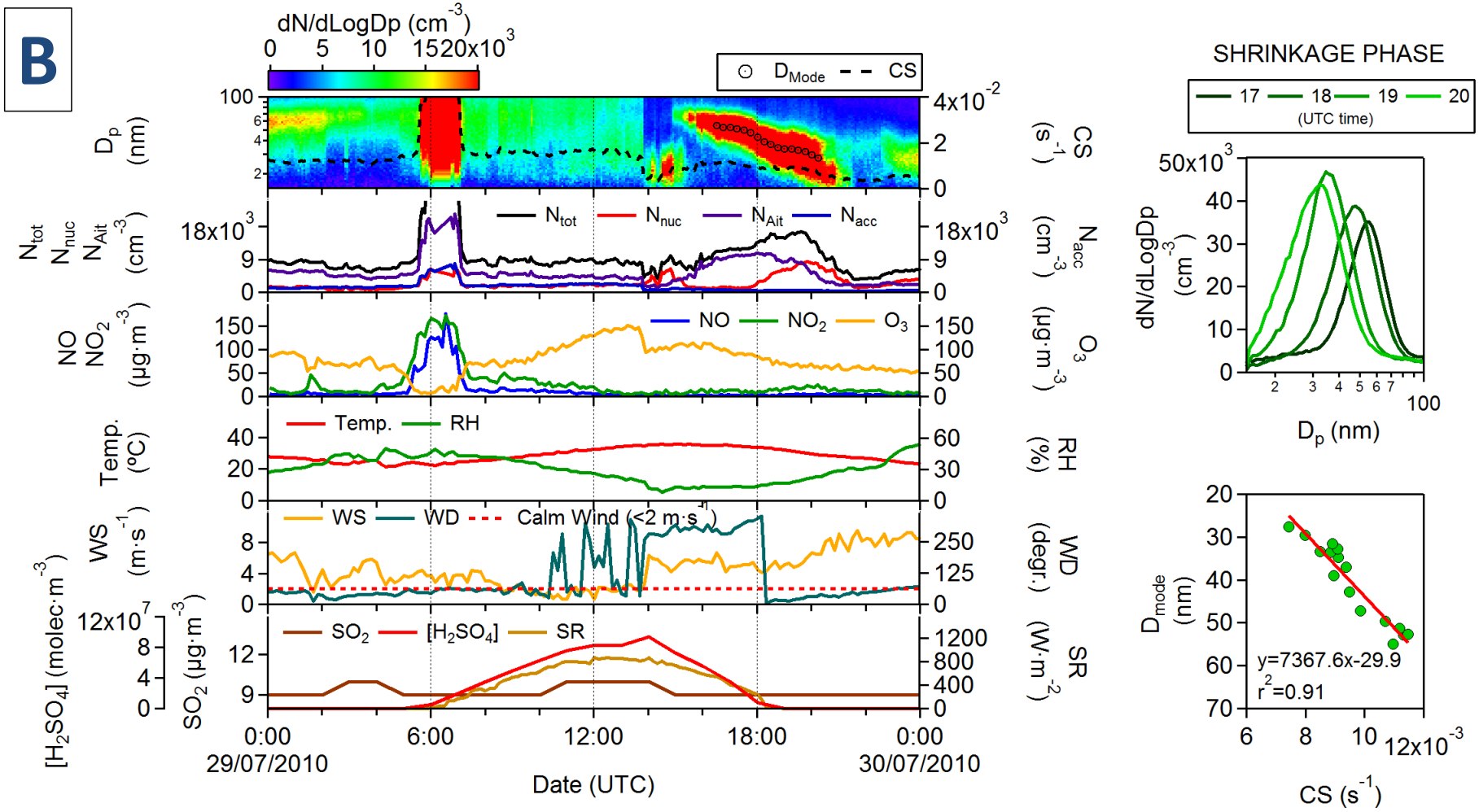
B
dN/dLogDp (cm-3)
0 5 10 1520x10^3
D_Mode
CS
D_p (nm)
CS (s-1)
N_tot N_nuc N_Ait (cm-3)
N_tot
N_nuc
N_Ait
N_acc
N_acc (cm-3)
NO NO2 (µg·m-3)
NO
NO2
O3
O3 (µg·m-3)
Temp. (ºC)
Temp.
RH
RH (%)
WS (m·s-1)
WS
WD
Calm Wind (<2 m·s-1)
WD (degr.)
[H2SO4] (molec·m-3)
SO2 (µg·m-3)
SO2
[H2SO4]
SR
SR (W·m-2)
0:00 29/07/2010
6:00
12:00
18:00
0:00 30/07/2010
Date (UTC)
SHRINKAGE PHASE
17 18 19 20
(UTC time)
dN/dLogDp (cm-3)
D_p (nm)
D_mode (nm)
y=7367.6x-29.9
r2=0.91
CS (s-1)

Fig. S3 Example of a complete study for each type of pure S event identified on A) 5 July 2013 (S event under a polluted air from traffic) and B) 30 July 2010 (S event under an air mass free of traffic emissions). Evolution of the aerosol size distributions and total (N_{tot}) and modal (N_{nuc}, N_{Ait} and N_{acc}) particle number concentrations in relation to air mass composition (SO_2, NO_x and O_3) and meteorological variables (Temp.=Temperature, RH=Relative Humidity, WS=Wind Speed, WD=Wind Direction, SR=Solar Radiation) are represented. D_{mode} estimation, gas-phase H_2SO_4 proxy value and CS have also been included. The gradual shift of 1-h average aerosol size distributions and the correlation between D_{mode} and CS is shown on the right side of the graph. Given that the site has a clean background, the time evolution of particle size distributions has been drawn up to 100 nm.

Table S1. Summary of the main characteristics (T: ambient temperature, RH: relative humidity, WS: wind speed, prevailing WD(s): prevailing wind direction(s), SI: solar irradiance) and calculated parameters (GR and SR: growth and shrinkage rates) for each case of NPF+shrinkage event identified at the CIEMAT site during 2009–2015. *NPF+shrinkage events in which several consecutive processes of growth and shrinkage occurred.

NPF+shrinkage events															
Day	NPF phase								Shrinkage phase						
	NPF type	Period	GR (nm h^{-1})	T (ºC)	RH (%)	WS (m s^{-1})	Prevailing WD(s)	SI (W m^{-2})	Period	SR (nm h^{-1})	T (ºC)	RH (%)	WS (m s^{-1})	Prevailing WD(s)	SI (W m^{-2})
17/07/2009	Ia	12:00-17:45	2.9	25.5±0.6	20±2	7.3±1.0	WNW	725±207	17:45-20:00	-7.6	24.2±1.1	20±2	5.4±1.8	NNE	53±92
18/07/2009	Ia	09:00-20:15	5.5	25.2±3.5	17±9	2.2±0.7	SSW-S	599±341	20:15-23:45	-2.6	25.2±1.0	20±5	3.7±1.3	ENE	0
17/05/2010	Ia	12:30-18:00	2.7	24.7±0.8	30±1	2.4±0.9	NNW-NW-WNW	658±232	18:00-22:00	-2.9	20.4±2.4	34±4	5.3±1.4	NE	8±22
19/05/2010	Ia	10:45-17:00	4.0	28.1±1.2	27±2	3.3±1.0	NNE-NE	788±156	17:00-21:00	-5.9	24.9±2.9	33±6	6.2±1.6	NNE	85±137
22/05/2010	Ia	11:15-16:45	2.4	28.3±1.3	26±3	2.4±0.5	WSW-W-SW	787±153	16:45-19:30	-2.1	28.2±1.2	24±2	2.3±0.5	SE-SSW-WSW	148±155
30/05/2010	Ia	10:00-20:15	4.7	29.1±1.7	32±4	2.8±1.3	NE-WSW-SW-NNW	554±363	20:15-21:00	-10.2	25.1±0.2	38±1	5.0±0.4	NE	0
06/06/2010	Ia	13:30-18:15	10.6	29.7±0.7	19±1	4.3±1.0	WSW-SW	546±262	18:15-20:45	-4.6	25.9±1.1	26±3	3.9±1.0	WSW-SW	19±29
06/07/2010	Ia	11:15-16:45	3.6	33.0±1.4	29±4	2.0±0.6	W-S	776±143	16:45-18:45	-4.5	34.4±0.3	24±1	2.0±0.5	W-WSW-SE-SSE	210±149
25/07/2010	Ia	09:00-16:15	5.9	29.4±2.7	24±2	2.1±0.6	NE-NNE	780±104	16:15-19:30	-5.2	31.4±1.5	18±1	5.8±1.7	NNE-NE	210±191
03/08/2010	Ia	09:45-19:45	4.6	28.8±2.3	24±10	2.2±0.7	ENE-NE-N-NNE	568±321	19:45-00:00	-4.9	25.9±1.9	52±9	6.9±1.0	NE-ENE	0
28/08/2010*	Ia	11:15-19:30	3.3	31.3±1.2	20±2	2.0±0.9	NE-ENE-NNE	492±326	19:30-20:45	-5.7	28.7±0.6	17±1	6.8±0.4	NE	0
		20:45-22:30	3.8	26.7±0.8	23±4	6.3±0.5	NE	0	22:30-23:45	-2.2	24.7±0.4	32±1	5.7±0.6	ENE-NE	0
14/05/2012*	Ia	10:30-14:30	4.5	28.0±0.9	20±4	6.6±1.7	WNW-W	888±37	14:30-15:30	-4.1	29.3±0.2	16±1	7.2±1.0	WNW	718±47
		15:30-17:15	1.5	28.7±0.4	18±1	8.3±0.9	NW-WNW	469±101	17:15-17:45	-1.8	27.8±0.2	20±1	8.9±0.7	WNW	249±38
		17:45-19:00	2.3	26.9±0.5	22±1	7.3±0.4	NW	26±57	19:00-19:30	-2.0	25.4±0.4	26±2	7.0±1.4	WNW	0
10/06/2012*	Ib	08:00-10:30	3.0	22.3±0.6	48±2	5.2±1.0	WSW-W	491±144	10:30-11:15	-2.4	22.8±0.1	47±1	5.2±0.6	WSW	301±131
		11:15-12:45	4.4	24.1±0.6	45±2	5.1±0.8	WSW	598±190	12:45-15:00	-7.3	25.3±0.7	41±3	5.5±1.0	W-WSW	399±125
30/06/2012	Ib	14:00-16:45	5.5	25.1±0.3	22±1	6.6±1.3	SW-NW-WNW	720±130	16:45-19:30	-6.7	24.1±0.9	22±3	6.2±1.1	NW-WNW	180±171
01/07/2012	Ia	11:15-15:45	7.2	23.5±1.3	23±3	2.8±1.1	WNW-NW-NNW-SW	799±206	15:45-19:45	-3.8	24.7±0.7	19±1	4.6±1.0	N-NNE-WNW	264±234
04/07/2012	Ib	12:00-16:15	7.1	29.6±0.5	20±2	6.3±0.7	WNW-W-NW-WSW	816±123	16:15-21:15	-1.5	27.8±1.9	21±4	6.0±1.2	NW	151±197
30/08/2012	Ib	10:30-16:45	2.8	28.5±1.4	19±4	2.2±0.8	N-NE-E	688±181	16:45-18:30	-3.8	26.9±1.8	26±4	8.3±1.2	NNE	76±109
03/05/2013	Ia	10:00- 18:15	1.4	16.3±1.5	40±4	597±330	N-NNE-NW	597±330	18:15- 20:00	-4.8	16.8±0.3	38±1	2.3±1.7	E	1±3

NPF+shrinkage events															
Day	NPF phase								Shrinkage phase						
	NPF type	Period	GR (nm h^{-1})	T (°C)	RH (%)	WS (m s^{-1})	Prevailing WD(s)	SI (W m^{-2})	Period	SR (nm h^{-1})	T (°C)	RH (%)	WS (m s^{-1})	Prevailing WD(s)	SI (W m^{-2})
04/05/2013	Ia	12:15- 17:45	1.6	19.6±1.0	29±2	662±231	WNW	662±231	17:45- 19:15	-4.0	19.7±0.4	30±1	3.0±0.3	SW-SSW	13±28
12/05/2013	Ia	11:15- 17:45	2.3	22.7±0.8	17±2	679±232	WSW-WNW	679±232	17:45- 19:00	-5.1	23.0±0.3	17±2	2.7±0.5	WSW	28±56
24/05/2013	Ia	12:45- 19:45	3.0	21.1±1.1	16±4	494±349	WNW	494±349	19:45- 21:15	-1.5	16.9±0.6	25±1	1.7±0.9	WNW, NW, NNW	0
03/07/2013	Ia	11:45- 17:30	5.8	32.5±0.9	17±2	651±256	NE-NNE	651±256	17:30- 0:00	-2.1	29.0±2.4	33±9	6.3±1.0	NNE-NE	25±69
04/07/2013	Ia	9:45- 17:15	6.3	32.3±2.3	22±7	762±156	NE-NNE	762±156	17:15- 21:30	-3.2	32.2±2.0	19±4	5.8±2.0	ENE	56±112
31/08/2013	Ia	11:45- 17:00	3.5	27.7±1.3	22±5	664±181	SE-SSE	664±181	17:00- 18:45	-2.3	28.6±0.5	18±0	2.6±0.5	SE	76±98
16/05/2015	Ia	8:15- 17:15	3.4	23.3±4.3	25±10	751±168	NE-ENE-NNE	751±168	17:15- 20:45	-4.9	24.7±1.8	17±2	5.6±1.1	ENE-NE	51±103
21/05/2015	Ia	9:15- 16:15	2.8	17.9±2.4	28±6	826±112	NNE-NE	826±112	16:15- 20:15	-3.9	19.7±1.8	22±3	5.3±1.2	NNE-NE	158±192
22/05/2015	Ia	11:00- 16:15	2.9	19.7±1.7	21±4	843±125	NE-ENE	843±125	16:15- 19:45	-2.5	20.3±1.2	22±3	6.1±1.3	ENE	182±196
26/05/2015	Ia	9:15- 15:45	6.6	23.2±2.7	25±7	836±88	NNE-NE	836±88	15:45- 21:45	-5.5	25.0±2.5	20±5	4.7±1.1	NNE-NE	155±215

790

Table 4S2. Summary of the main characteristics (T: ambient temperature, RH: relative humidity, WS: wind speed, prevailing WD(s): prevailing wind direction(s), SI: solar irradiance) and calculated parameters (GR and SR: growth and shrinkage rates) for each case of growth process+shrinkage event identified at the CIEMAT site during 2009–2015. *Growth process+shrinkage event which showed a bi-modal size distribution.

Growth process+shrinkage events														
Day	Growth phase							Shrinkage phase						
	Period	GR (nm h^{-1})	T (°C)	RH (%)	WS (m s^{-1})	Prevailing WD(s)	SI (W m^{-2})	Period	SR (nm h^{-1})	T (°C)	RH (%)	WS (m s^{-1})	Prevailing WD(s)	SI (W m^{-2})
29/07/2009	17:00-17:45	9.4	33.3±0.4	7±1	6.6±1.6	NW-WNW	344±53	17:45-19:45	-5.0	31.0±1.1	11±2	7.2±1.2	NW	50±89
31/07/2009	19:00-20:30	4.4	31.1±0.7	14±0	5.7±0.6	WSW-SW	0	20:30-22:45	-6.9	28.3±0.9	20±3	3.0±1.4	W-WNW	0
18/05/2010	19:45-21:00	3.6	21.3±0.5	29±1	6.0±0.5	NE	0	21:00-22:15	-3.2	20.0±0.3	32±1	6.8±0.3	NE-NNE	0
31/05/2010-01/06/2010	13:00-19:30	2.8	32.3±1.3	28±3	2.7±1.5	NE-N	486±334	19:30-02:30	-3.3	24.0±2.2	50±7	4.8±0.8	NE-ENE	0
22/06/2010	13:45-18:15	4.5	29.3±0.5	23±1	2.2±0.7	WSW-W	569±229	18:15-19:45	-2.3	29.0±0.7	22±1	2.7±0.9	SSW-SSE	0
27/07/2010*	12:00-17:30 (Mode 1)	3.7	32.0±1.4	22±4	1.8±0.6	SSW-SW-SE	684±192	17:30-20:45	-3.0	32.5±0.8	18±1	2.0±0.8	SSE	48±89
	12:00-17:45 (Mode 2)	5.6	32.1±1.4	22±4	1.8±0.6	SSW-SW-SE	660±212	17:45-20:45	-2.3	32.4±0.8	18±1	2.0±0.8	SSE	25±57
06/07/2011	16:15-18:00	4.2	30.7±0.2	15±1	6.5±0.5	WSW-SW	420±106	18:00-22:15	-4.7	27.1±2.0	15±47	5.7±1.6	WSW-W	19±4
05/06/2012	22:00-22:30	4.5	24.4±0.2	35±1	5.5±0.7	WNW	0	22:30-00:00	-4.7	23.4±0.5	41±4	4.4±0.3	WNW	0
14/06/2012	21:00-22:30	4.5	23.6±0.5	31±4	3.4±0.6	W	0	22:30-00:45	-6.0	21.9±0.5	40±1	3.9±0.9	W-SW-WSW	0
21/04/2013	17:15- 19:45	3.3	13.1±0.6	50±2	1.2±0.9	NNE	9±18	19:45- 23:15	-2.2	11.7±0.5	53±2	3.7±0.8	NNE	0±0
23/06/2013	13:30- 14:45	3.9	30.0±0.3	19±1	4.0±0.6	W-NNE	640±140	14:45- 19:15	-6.2	28.2±1.4	15±2	6.3±1.1	NNE	181±166
25/06/2013	20:00- 21:15	6.5	27.2±0.8	18±3	6.2±1.8	NE	0±0	21:15- 0:00	-5.2	22.5±1.5	36±5	8.8±0.8	NE	0±0

Table ~~5~~S3. Summary of the main characteristics (T: ambient temperature, RH: relative humidity, WS: wind speed, prevailing WD(s): prevailing wind direction(s), SI: solar irradiance) and calculated parameters (SR: shrinkage rate) for each case of pure shrinkage event identified at the CIEMAT site during 2009–2015. *Day in which two shrinkage events occurred.

Pure shrinkage events							
Day	**Period**	**SR** ($nm \cdot h^{-1}$)	**T** (°C)	**RH** (%)	**WS** ($m\ s^{-1}$)	**Prevailing WD(s)**	**SI** ($W\ m^{-2}$)
03/07/2009	17:30-21:00	-10.5	30.4±1.3	24±3	8.7±0.8	WSW	67±116
08/07/2009	21:45-23:30	-11.1	24.4±1.4	38±4	8.4±1.6	NE	0
13/07/2009	20:45-00:00	-4.2	27.4±1.0	26±2	4.8±1.0	WNW	0
29/08/2009	20:15-22:15	-11.1	29.0±0.5	24±1	5.3±0.9	ENE-NE	0
14/06/2010	18:00-22:00	-1.6	19.7±1.9	50±7	5.8±1.8	NE	24±57
24/06/2010	13:15-17:45	-2.5	31.9±0.5	21±1	2.4±0.9	SSW	570±177
05/07/2010	21:30-00:00	-4.7	26.9±1.0	38±0	6.3±0.6	NE	0
25/07/2010	21:00-23:30	-5.1	24.7±0.7	30±3	8.0±1.1	NE	0
29/07/2010	16:15-20:15	-7.3	32.8±2.0	16±3	5.3±0.7	WNW-NNE	184±208
04/08/2010	15:30-00:00	-3.0	28.4±2.5	29±5	4.5±1.2	NE-ENE-WNW-NNE	101±164
29/08/2010	16:15-22:45	-6.4	29.0±2.6	22±2	4.6±1.4	NW-NE-WNW-ENE	60±122
30/08/2010	17:30-00:00	-2.2	27.4±2.8	17±7	5.7±0.8	NNE-NE	5±19
09/05/2011	14:30-17:15	-2.7	24.7±0.3	22±1	2.5±0.7	SW-WSW	433±233
07/07/2011	16:00-19:30	-1.7	26.0±1.1	18±1	8.0±0.8	NW	265±221
06/06/2012	16:15-23:45	-3.1	25.8±2.1	37±8	6.0±2.5	WSW-SW	98±178
29/06/2012	16:30-20:15	-2.6	27.0±1.1	20±3	7.2±0.9	WSW-SW	179±201
05/07/2012	16:30-19:45	-2.9	25.5±0.8	18±2	7.8±0.8	NW	203±201
13/07/2012	19:15-23:45	-7.8	26.8±2.2	33±9	5.8±0.6	WNW-NW	0
14/07/2012	14:30-22:30	-1.0	26.5±2.3	16±3	4.8±1.3	NW-WNW-NNW	242±290

Pure shrinkage events							
Day	**Period**	**SR** ($nm \cdot h^{-1}$)	**T** (°C)	**RH** (%)	**WS** ($m \cdot s^{-1}$)	**Prevailing WD(s)**	**SI** ($W \cdot m^{-2}$)
15/07/2012	19:45-22:30	-8.6	26.1±1.4	20±4	7.4±1.9	NE-ENE	0
21/07/2012*	17:30-20:45	-7.2	31.3±1.4	21±2	4.7±1.0	NNW-NW	63±111
	20:45-22:45	-8.2	27.1±1.0	27±2	7.8±1.2	ENE-NE	0
22/05/2013	20:15- 22:15	-1.9	16.1±0.6	44±2	5.7±1.2	NE-NNE	0±0
25/05/2013	19:30- 23:15	-1.7	17.4±1.6	30±5	6.4±1.6	NE-ENE	0±0
05/07/2013	19:15- 22:45	-3.8	31.3±1.5	20±2	5.6±0.6	SSE	0±0
25/08/2013	17:45- 21:30	-9.2	27.5±1.7	20±2	4.6±1.2	NW-NE	5±17
15/05/2015	15:00- 20:45	-1.1	20.3±1.8	31±5	7.7±1.0	NE	245±266
19/06/2015	18:00- 0:15	-4.9	25.7±3.0	29±6	6.9±1.7	ENE-NNE-NE	7±32
08/07/2015	21:15- 1:00	-2.6	27.6±1.6	34±4	6.6±1.7	NE-ENE	0±0
15/09/2015	2:15- 9:00	-2.3	15.2±0.5	53±1	5.1±1.5	SSW-SW	62±125

799

800